UNIVERSITA' DELLA CALABRIA
Dipartimento di Farmacia e Scienze della Salute e della Nutrizione

Scuola di Dottorato
SCIENZA E TECNICA "BERNARDINO TELESIO"

Indirizzo
Materiali organici di interesse farmaceutico

La presente tesi è cofinanziata con il sostegno della Commissione Europea,
Fondo Sociale Europeo e della Regione Calabria

CICLO
XXVII

MULTIVARIATE CURVE RESOLUTION METHODOLOGIES IN PHOTOSTABILITY DRUG STUDIES

Settore Scientifico Disciplinare CHIM/08

Direttore: Ch.mo Prof. (Roberto BARTOLINO)
Firma _____

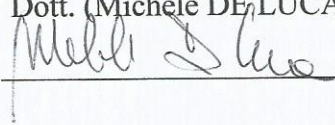**Coordinatore:**   Ch.mo Prof. (Bartolo GABRIELE)
Firma _____

Supervisore: Ch.mo Prof. (Gaetano RAGNO)
Firma _____

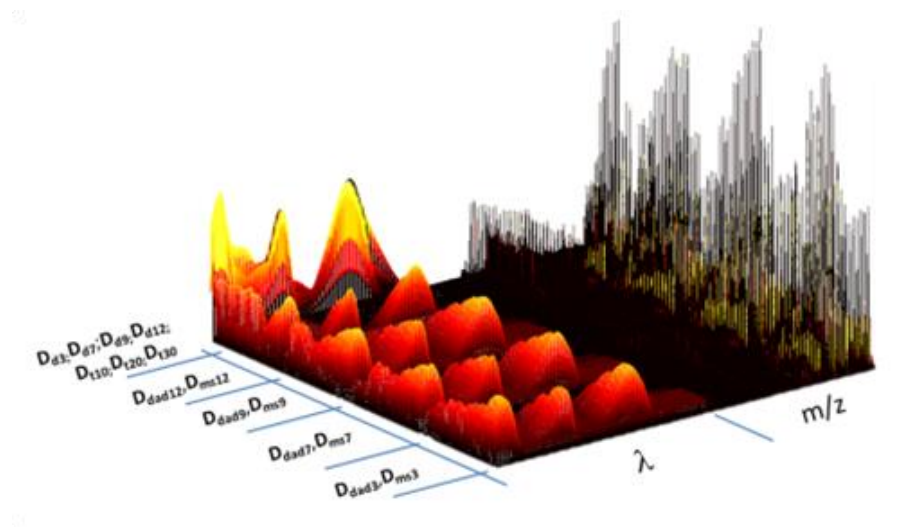**Dottorando:** Dott. (Michele DE LUCA)
Firma _____

To my Family

INDEX

MULTIVARIATE CURVE RESOLUTION

METHODOLOGIES IN PHOTOSTABILITY DRUG STUDIES

INTRODUCTION

Pharmaceutical analysis embraces all the aspects of the in-process and quality control testing of drug substances and their formulated products. It indeed plays a crucial role in the identification of new targets, activity evaluation, pharmacokinetics and biotransformation, quality control, stability and formulation studies (Berridge et al., 1991).

Pharmaceutical analysis is assuming a fundamental role not only in the quality control of already existing drugs but, in the last years, has evolved in combined analytical techniques, high-throughput technologies, chemometrics and nanotechnology (Koh et al., 2003; Albert et al., 2002; Sweedler, 2002).

The United State FDA is in the forefront of this change with its PAT initiative (Process analysis technologies), inviting the pharmaceutical industry to convert to modern process monitoring based on timely and multi-dimensional analysis in the whole of production, optimizing the process and minimizing the fault risk (Wold et al., 2006).

In the last years, light has been recognized as one of the most important factors, together with heat, humidity and pH, involved in drug degradation. Research on similar problem has not yet been widely developed, despite the large number of light sensitive drugs and excipients. However, the drug photostability studies are actually part of a general drug monitoring program which mostly consists of researching the causes of drugs decomposition, determining the pathway of kinetic process, and selecting the suitable tools able to reduce the degradation. In this context, the loss of drug activity is not allowed when the biological or therapeutic effect is going to be modified or when general toxicity is going to be enhanced (Ragno et al., 2006a; Ragno et al., 2006b).

In 1991, a detailed guide for stability studies on new drugs has been issued by ICH (International Conference on Harmonization), being recommended in Europe, Japan and USA, and at least consulted all over the world. Such direction specifies the required information for the registration of new molecules and mixtures in pharmaceutical products. The best up-to-date pharmaceutical legislations, among general dispositions, prescribes that a request for the introduction of a new

formulation is accompanied with a so-called "stability report". In this context, a light exposition test is considered fundamental during the entire process (ICH, 1991).

Methods of analysis have changed in recent years with more use of instrumental techniques, able to generate large data sets. Chemometrics has allowed the description and rationalization of many analytical systems, by means of the simultaneous use of a very high number of signals.

PAT protocol reports the use of chemometric methodologies in the critical control points in pharmaceutical manufacturing (Wold et al., 2006):

- calculating concentrations and other properties from spectral data by multivariate calibration;

- classifying samples (active pharmaceutical ingredients, excipients, intermediates, final products) as acceptable or not, based on spectra or/and property profiles;

- monitoring the evolution of a batch process by means of multivariate measurements (process data and spectra) and using the process and raw material data to classify the process as acceptable or not;

- combining data from several or all critical process steps and raw materials to assess quality of the final product.

The multivariate modeling evolves through a series of steps: design of the experiments, data making, data pre-treatment, modeling, optimization and validation. Each of these is important and last researches in chemometric field are focused to find new methodologies and/or algorithms to improve the multivariate modeling performance. The description of the exact photochemical behavior of a specific molecule is really difficult, as Grenhill has pointed out in a review in 1995 (Greenhill et al.,1995). This is due to the fact that the photodegradation mechanism depends on a complex way on the structure and on experimental conditions and then the

kinetics and photoproducts distribution may significantly vary even among closely related compounds (Albini et al., 1997).

Multivariate Curve Resolution - Alternating Least Squares (MCR-ALS) is one of the recent chemometric techniques frequently used for the analysis of spectrophotometric data (Javidnia et al., 2008; de Juan, et al., 2000). It is able to resolve the different sources of variance in a data set and allows the study of complex evolving chemical processes, as a degradation, estimating the number of components, their pure spectra and their concentration profiles. When the investigated process is a kinetic reaction, it allows also the estimation of rate constants (k) (De Luca et al., 2010).

This thesis contains a detailed report about research methodologies and results achieved in my Doctoral School. The main topic of this investigation has been focused on the study of drug photostability by using different experimental and analytical procedures. The degradation kinetic processes have been studied by applying modern chemometric methodologies. During my research stage in Spain, I have had the opportunity to collaborate with one of the most important research groups in chemometrics, headed by Prof. Romà Tauler (Department of Environmental Chemistry - Institute of Environmental Assessment and Water Research CSIC - Barcelona). In that period, I had the possibility to develop and apply new chemometric algorithms able to study in depth the photostability of drugs and pharmaceutical matrices.

1. DRUG PHOTODEGRADATION STUDIES

The photostability of drugs is a fundamental topic in the pharmaceutical investigation. The importance of drug photostability has been recognized only in the last decades of the twentieth century, whereas up to that time the matter had played a less important role in the field of technological and analytical pharmaceutics. Contemporarily, the new international pharmacopoeia versions introduce the first rules, or advices, to minimize the effects of the light. These rules just recommended the maintenance of the drugs or drug formulations in containers resistant to light (Tønnesen, 2001; Beijersbergen Van Henegouwen, 1997).

Nowadays, light irradiation has been recognized as one of the most important parameter for drug stability evaluating and new pharmaceutical compounds are regularly added to the list of photolabile drugs (Tønnesen, 2004). Drug degradation can lead loss of biological activity, but in several cases toxic degradation products are produced. The exposure to sunlight can cause sunscreens photodegradation and determine their decrease in UV protection often with the occurrence of allergic and/or toxic degradation products (Periolia et al., 2006). Photo-transformation products of naproxene were demonstrated more toxic than the parent compounds both for acute and chronic values, while genotoxic and mutagenic effects were not found (Isidori et al., 2005). Systemic toxic effects resulting from photoactivation of nitroaromatics, as nifedipine, should be considered as a possibility (de Vries and Beijersbergen van Henegouwen, 1998). Tretinoin and isotretinoin undergo complete isomerization just within a few seconds of light exposure to give 13-cis and 9-cis isomers, respectively. Teratogenicity for isotretinoin is well documented (Kochar et al., 1984; Hixson et al., 1979) and it is suspected as a potential effect for tretinoin. For these reasons,

actually, the use of tretinoin in pregnancy is forbidden (Ioele et al., 2005). The European Pharmacopoeia declares warnings for light exposure about more than 300 medical substances and new compounds are frequently added to this list.

A high number of kinetic degradation has been postulated in scientific articles and books about photochemistry (Horspool and Song, 1995; Kopecky et al., 1992; Coyle et al., 1982). The studies concerning the prediction of the photochemical behaviour of new drugs on the basis of its molecular structure seems as well interesting, but the published articles about are few (Hatipoglu and Çinar, 2003; Hemmeteenejad et al., 2002; Andreazza Costa and Gaudio, 1997).

Molecular degradation caused by the light can also occur after drug administration and photoproducts can interact with endogenous molecules giving biological effects. (Song and Tapley, 1979; Rahn et al., 1974).

The study of photoreactivity of a drug is nowadays counted on when its global profile is defined. A basic protocol for testing the photostability of new drugs is described in the ICH Guideline, as part of the essential drug stress testing activities in the pharmaceutical industry (ICH, 1991). The intrinsic photostability characteristics of new drugs should be evaluated to demonstrate that, as appropriate, light exposure does not result in unacceptable changes. The impurities from synthesis and degradation must be identified and quantified and their limits have to be established. When necessary, the toxicological aspects of these impurities must be defined through specific studies.

1.1.   Photostability test on drug compounds.

The interest for the drug photostability is of recent interest and therefore the rules concerning the test to perform on new drugs have been established just in the last years.

The institute ICH (International Conference on Harmonization) has prepared the first compilation of a full rational program containing the rules for the stability control of the drugs (Drew, 1998; Helboe, 1998; ICH, 1991). The guide "Stability Testing New of Drugs Substances and Pharmaceuticals" has been adopted in 1996 in the European Community and in 1997 in USA and Japan. The ICH rules note that light testing should be an integral part of the global stress testing performed on new pharmaceutical compounds. The ICH rules include photostability tests on both pure drug and their pharmaceutical forms. Similar tests on the commercial products are required, as on the immediate pack as on the marketing pack. The use of the solar radiation is of course not advisable because of its dependence from the geographical position and weather conditions (Anderson and Byard, 2004; Moore, 2004).

Photostability tests can be performed by using two different light sources:

• Option 1: the samples are irradiated under a light source producing an output similar to the D65/ID65 emission standard. An artificial daylight fluorescent lamp combining visible and ultraviolet (UV) outputs, xenon, or metal halide lamp are suitable for this test. D65 is the internationally recognized standard for outdoor daylight as defined in ISO 10977 (1993). ID65 is the equivalent indoor indirect daylight standard. If necessary, appropriate filters must provide to eliminate the radiations below 320 nm.

• Option 2: a cool white fluorescent and a near ultraviolet lamp are both required. The first must produce an output similar to that specified in ISO 10977

(1993); the second lamp must furnish a spectral distribution from 320 nm to 400 nm with a maximum energy emission between 350 nm and 370 nm.

This accurate definition of the light sources has been helpful to avoid different procedures in the photostability tests. Whatever the option is chosen, the operator should mind to maintain an appropriate control of the temperature to minimize the effect of localized temperature changes caused by the light sources.

1.2. Natural and artificial sources.

During production, packaging and consumer handling, pharmaceutical products can be exposed to light from different sources, ranging from natural sunlight to a variety of artificial light conditions. In terms of the probability of photochemical interaction, the UV contribute of sunlight is the most potentially damaging. However, long periods of exposure to fluorescent or incandescent lighting can give enough
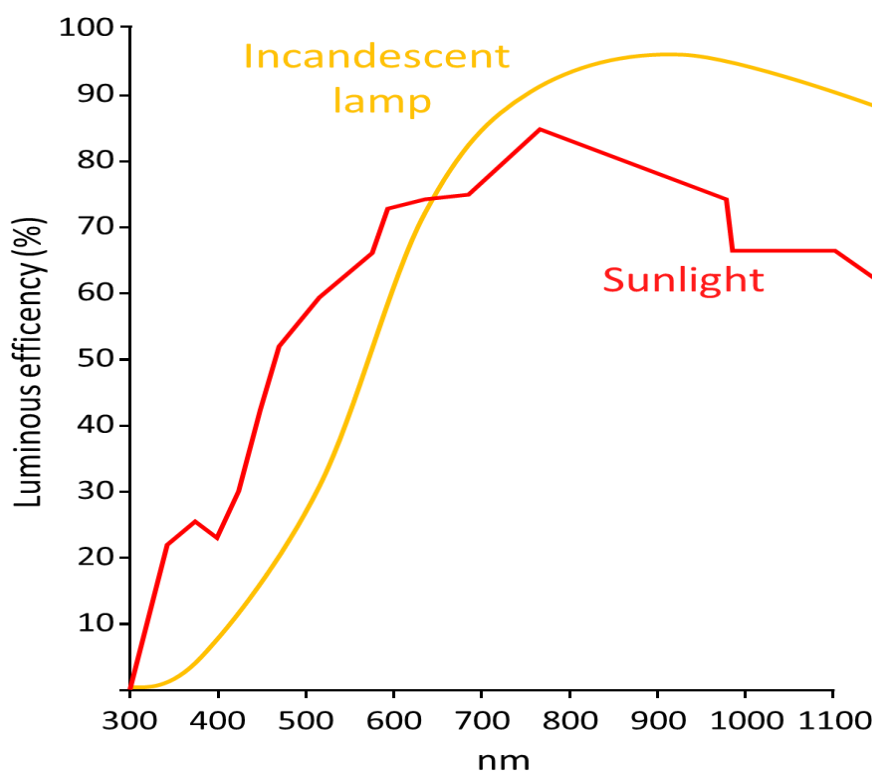

Figure 1.1 - Spectral power distribution of sunlight compared with an artificial source.

energy to start a photodegradation reaction. Relative spectral intensity curves are shown in Figure 1.1 for sunlight and an incandescent (filament) lamp. Each of these spectra extends from near 300 nm in the ultraviolet region to beyond 3000 nm in the infrared, but with differing intensity distribution.

UV radiation consists of three sub-bands: UVC, UVB, and UVA (Grossweiner, 1989). The UVC (or far-UV) band is between 200 to 280 nm and many drugs and cellular constituents absorb UVC, however, sunlight at the Earth's surface does not contain UVC because of atmosphere screen (Frederick et al., 1989). UVC is present in artificial radiation sources, such as discharge and germicidal lamps and welding arcs, and can cause rapid photochemical degradation, as well as serious damage to the skin and cornea following exposure (Cadet et al., 1992). The UVB spectral region is from 280 to 320 nm (Grossweiner, 1989). The DNA and the aromatic amino acids are the major cellular absorbers of UVB and it is known that UVB can cause sunburn, skin cancer, and other biological effects and is responsible for the direct photoreaction of many chemicals in natural sunlight (Epstein, 1989). The UVB intensity at a particular latitude varies greatly with time of day and the season of the year, as the variation of the solar azimuthal angle varies the path length of the sun's rays through the stratospheric ozone layer. UVA (near-UV) is the UV region from 320 to 400 nm. The amount of solar UVA reaching the Earth's surface is greater than that of UVB (Gates, 1966). Chemical and biological effects induced by UVA may involve direct energy absorption of proteins and DNA and endogenous or exogenous substances. Artificial light sources can have varying spectral characteristics depending on the particular construction. The key component of a fluorescent light is the low pressure mercury discharge at 254 nm within a glass tube coated internally with a phosphor having specific emission characteristics. Although the principal output is in the visible region, there is a significant UV component.

1.3.   Light absorption of a drug.

The energy of a photon at 300 nm is about of 400 kJmol^{-1}, which equals to the bonding energy of an organic compound.

If a drug can absorb radiations in ultraviolet or visible wavelength range, the absorbing energy could be sufficient to break molecular bonds. Thus, the property absorption of a drug is an indication of the photosensitivity and possibility of photodegradation.

The photochemical reaction must follow the basic law of photochemistry (Grotthus and Draper in 1818), where photochemical reaction can occur only with electromagnetic radiation absorption. When drug compounds are coloured, they absorb light in the visible region and the displayed colour is complementary to the absorbed light. Most of the drugs are white coloured and do not absorb in the visible region, but they may absorb in the UV region in accordance with the chemical structure. Aromatic groups and conjugated double bonds with N, S, or O in the structure are usually matched with the light absorption properties of the molecules.

2.   CHEMOMETRIC METHODOLOGIES

All phenomena are multivariate and this means that any analytical problem we want to study depends on several factors. For instance, the human health depends on several variables, including genes, social habitat, eating habits, stress, physical activity and so on.

Any chemical process is a complex data system and it is essential to know what to measure and how and where to sample, and then to study a certain domain in an abstract multidimensional space. The coordinates of this space are partly known, and partly unknown, because we do not know fully how to represent a chemical problem. A series of experiments are need to find the best set of conditions inside this domain. Moreover, further experiments are needed to study, interpret, and understand the variation of properties in this domain. Empirical models are necessary to connect the experimental results (data), because theory takes us only to the boundaries of this domain. Of course, these empirical models need to be consistent with the theory, at least on the boundaries of the domain. Experimental design helps to investigate this domain magnitude in a more efficient mode, obtaining so more analytical information against the traditional 'one factor at a time' approach (Ruckebusch and Blanchet, 2013).

"Chemometrics is a chemical discipline that uses mathematics, statistics and formal logic (a) to design or select optimal experimental procedures; (b) to provide maximum relevant chemical information by analyzing chemical data; and (c) to obtain knowledge about chemical systems" (Massart etal., 1997).

The amount of information available from the analytical measurements has increased greatly in recent years, so methods to solve complex information content

are important. Chemometrics has become a very important tool because it allows to process and interpret large amounts of information content in chemistry analytical data (Hanrahan, 2009). Principal Component Regression (PCR) or Partial Least Squares (PLS) are the most known methods (Hanrahan, 2009). When the data have nonlinear concentration of analytes, other methods such as Artificial Neural Network (ANN) or Least-Squares Support Vector Machine (LS-SVM) can be used (Suykens, 2009). In all cases, the construction of a set of calibration samples representative of the variability of the unknown samples is required and validation of the model obtained with a set of appropriate prediction samples has to be performed.

For second order data, there are more sophisticated methods such as Parallel Factor Analysis (PARAFAC, Bro, 1997), Generalized Rank Annihilation Method (GRAM, Sanchez, 1986), Direct Trilinear Decomposition (DTLD, Sanchez, 1990) or Multivariate Curve Resolution-Alternating Least Squares (MCR-ALS, Tauler, 1995), particularly relevant for the analysis of complex mixtures. Other methods widely used to analyze second order data are: Principal Component Analysis (PCA) or methods usually called Factor Analysis (FA, Hopke, 2009), pattern recognition methods (Pattern Recognition, Hopke, 2009b), Cluster Analysis (CA Bratchell 1989) or Discrimant Analysis (DA, Lavine, 2009). For higher order data, methods such as PARAFAC, TUCKER3 (Tucker, 1966) or MCR-ALS are used.

2.1. Mutivariate Curve Resolution

When a chemical process is monitored by instrumental analysis, a series of signals are collected and stored, furnishing the temporal evolution of the system. These data contain the information about all species involved in the chemical process. The characterization of the various components in a chemical process represents a serious analytical problem because the resolution depends on the

complexity of the system, the overlap of the spectra and the number of the involved species. These difficulties increase in the presence of interferences that are rapidly transformed and their concentration profiles are merged with those of reagents and products. Chemometric methods have been proposed to resolve such complex multicomponent systems such as the MCR-ALS method (de Juan and Tauler 2006).

MCR-ALS is based on a bilinear modelling which decomposes the experimental data into the concentration and signal or spectral contributions of the pure components present in the analysed complex system or evolving during a particular chemical process (Hemmateenejad et al., 2008; Kessler et al., 2006). This bilinear decomposition on pure component contributions can be described according to the following equation:

1) $\mathbf{D} = \mathbf{C}\,\mathbf{S}^T + \mathbf{E}$

In the rows of the experimental data matrix $\mathbf{D}$ there are the experiments collected at different reaction times or samples and in the columns there are the signals at the different variables (wavelengths, mass unit, ect) evolving with the experimental procedure. $\mathbf{C}$ is the concentration matrix of the n components involved in the process, $\mathbf{S}^T$ is the spectral matrix of the pure components and $\mathbf{E}$ contains the unexplained data variance. This model is analogous to the multi-wavelength and multi-sample extension of Lambert-Beer's law (Skoog and West, 2004).

In the MCR applications, the first step is the estimation of the number of components, which may be simply performed through a chemical rank (mathematical rank in absence of noise) analysis of the data matrix $\mathbf{D}$. Principal component analysis (PCA) and singular value decomposition (SVD) (Golub and Van Loan, 1989) can be used for this purpose. MCR-ALS also requires an initial estimate of either $\mathbf{S}^T$ or $\mathbf{C}$

matrix, which can be obtained by selection of the purest variables (rows or columns) of the data matrix **D** (Windig and Guilment, 1991; Gampp et al., 1987). These initial estimates are then optimized using an Alternating Least Squares (ALS). At each iterative cycle, a new estimation of S^T or **C** are obtained solving alternatively equation 1 for these two unknown matrices. In absence of constraints, the linear least-squares solutions of equation 1 are given by the matrix equations:

2) $S^T = (C)^+D$

3) $C = D(S^T)^+$

where $(S^T)^+$ and $(C)^+$ are the pseudoinverses of S^T and **C** matrices, respectively. In order to have MCR solutions with physical meaning, constraints are applied to **C** and S^T matrices during the ALS procedure (Golub and Van Loan, 1989).
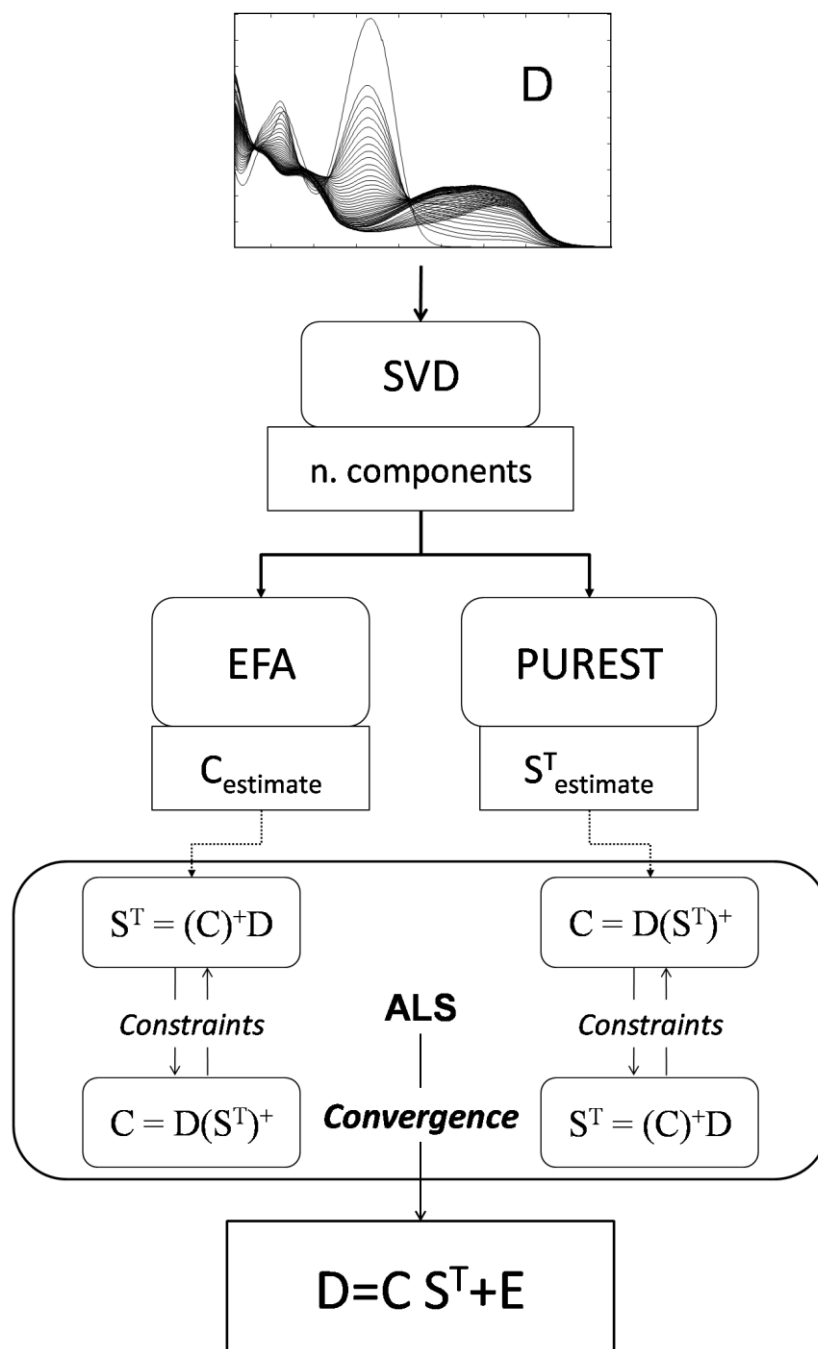
Figure 2.1 - Flow chart of the Multivariate Curve Resolution-Alternating Least Squares (MCR-ALS) procedure.

The constraint more commonly used for absorption spectroscopic data is the non-negativity constraint, for both concentration and spectra profiles (matrices **C** and **S**^{T} in equation 1). This can be achieved applying non-negative least squares

procedures for solving equations 2 and 3. Other constraints like unimodality on peak shaped profiles or closure for the fulfilment of mass-balance equations can be also applied. See references for more details about constraints implementation and examples of their application (de Juan et al. 1997; Gargallo et al., 1995). Figure 2.1 shows the flow chart of the Multivariate Curve Resolution-Alternating Least Squares (MCR-ALS) procedure. The ALS iteration procedure is stopped when convergence is achieved, by fixing a preselected number of cycles or by evaluating the value of lack of fit (%lof). Another parameter commonly used to indicate the quality of MCR-ALS modelling is the percentage of explained variance (%R^2) (Tauler et al., 1995, Tauler, 1995). Their mathematical equations are listed below:

4) $\quad \%lof = 100 \times \sqrt{\dfrac{\sum_{ij}(d_{ij} - d_{ij}^*)^2}{\sum_{ij}d_{ij}^2}}$

5) $\quad \%R^2 = 100 \times \dfrac{\sum_{ij}d_{ij}^{2*}}{\sum_{ij}d_{ij}^2}$

MCR-ALS presents also the feature that allows the simultaneous analysis of multiple data sets, obtained from independent experiments at different experimental conditions and/or using different analytical and instrumental techniques. In this case, the whole data set are arranged in a column-wise augmented data (Garrido et al., 2005):

6) $\quad \mathbf{D}_{aug} = [\mathbf{D}_1;\ldots;\mathbf{D}_N] = [\mathbf{C}_1;\ldots;\mathbf{C}_N]\mathbf{S}^T + [\mathbf{E}_1;\ldots;\mathbf{E}_N] = \mathbf{C}_{aug}\mathbf{S}^T + \mathbf{E}_{aug}$

In equation 6, column wise matrix augmentation is shown by using the MATLAB semicolon notation ';'. This notation indicates that every individual $\mathbf{D_i}$ matrix (i=1,…,N), obtained in a different experiment, is arranged one on the top of the other, keeping the same number of columns (for instance, wavelengths) in common, and consequently increasing the number of spectra rows of the corresponding augmented matrix $\mathbf{D_{aug}}$ = [$\mathbf{D}_1$;…;$\mathbf{D}_N$].

The same spectral matrix $\mathbf{S}^T$ is resolved for all the $\mathbf{D_i}$ matrices. In contrast, every $\mathbf{C_i}$ concentration profile matrix in [$\mathbf{C}_1$;…;$\mathbf{C}_N$] (i=1,…,N), is coupled to a different experiment.

A detailed description of MCR methodologies, possible applications and new algorithms will be displayed in the next studied cases.

3. PHARMACEUTICAL SYSTEMS INVESTIGATED

3.1. Lonidamine and related impurities: HPLC analysis, stability profile and degradation pathways.

Lonidamine (LND) or 1-(2,4-dichlorobenzyl)-1H-indazole- 3-carboxylic acid, is an antispermatogenic drug (Silvestrini et al., 1984) and an anticancer (Silvestrini, 1991) currently used to treat a number of tumors, including head, neck (Magno et al., 1994), and breast (Amadori et al., 1998) cancers. The drug causes only minor signs of toxicity such as myalgia, asthenia, testicular pain, and gastrointestinal discomfort (Robustelli della Cuna and Pedrazzoli, 1991, Rosso et al., 1991). Even if the mechanism of action is still not completely understood, it is believed that this drug would not induce myelo-suppression and other typical side effects of the classic cytotoxic drugs because it would interfere with cell energy processes, by inhibiting aerobic glycolysis in cancer cells. Interestingly, it seems to enhance aerobic glycolysis in normal cells, but suppress glycolysis in cancer cells. This is most likely through the inhibition of the mitochondrially bound hexokinase. Later studies in Ehrlich ascites tumor cells showed that LND inhibits both respiration and glycolysis leading to a decrease in cellular ATP (Pelicano et al., 2006). LND has been shown to enhance the antitumor and cytotoxic effects of hyperthermia (Bloch et al., 1994), photodynamic therapy, several antineoplastic alkylating agents and adriamycin (Shevchuk et al., 1996). The recent studies about the pharmacological activities of LND have been reported in a recent review (Gatto et al., 2002).

The synthesis of the drug is depicted in figure 3.1 and is based on the alkylation of indazole-3-carboxylic acid (ICA) with 2,4 dichloro-benzyl chloride (DBC) (Corsi et al., 1976).
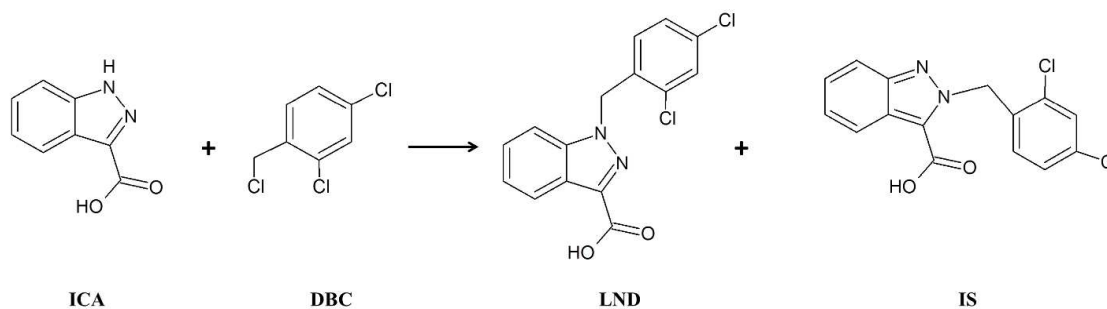
Figure 3.1 - Synthesis scheme of Ionidamine

Some secondary products can be obtained from this process. The most important is the 2N substituted isomer of LND, the 2-(2,4-dichlorobenzyl)-2H-indazole-3-carboxylic acid (IS). The parent substances ICA and DBC could also be potential impurities because their incomplete reaction.

In recent times, there is an increased tendency towards the development of stability-indicating assays (Ivana et al., 2006; Mohammadi et al., 2006; Singh et al., 2006), using the approach of stress testing as enshrined in the International Conference on Harmonization (ICH) guideline Q1AR(2) ICH, Q1A(R2). This guideline addresses the evaluation of stability data that should be submitted in registration applications for new drugs and associated drug products and provides recommendations on establishing re-test periods and shelf lives.

LND has been determined in human plasma and urine (Leclaire et al., 1983) and in serum (Bottalico et al., 1995), but at our knowledge, no report about a complete purity assay of LND has been published. Two papers dealing with the simultaneous determination of the drug and its isomer IS have been reported

(Vetuschi et al., 1989; Vetuschi, 1989) but no stability-indicating method has been reported. For this purpose, in the present work, the analytical profile of LND was studied in depth including its behavior when exposed to high temperatures or light. In literature, only a study describing the potential phototoxic properties of LND has been reported (Chekulayev et al., 1997). Since the indazole carboxylic acids are known to undergo easy decarboxylation, the presence of indazole (IND) and the decarboxylated form from LND (LDC) were monitored in the degraded samples of LND.

The photodegradation studies were conducted in accordance with the recommendations of the ICH rules by performing the stressing tests by means of a cabinet equipped with a Xenon lamp, able to adopt different irradiation modes reported in the ICH guide.

Identifying drug degradation products in LND formulations is of critical interest to ensure product quality with a significant impact on safety and efficacy of the drug. Degradation products formed from LND subjected to forced-degradation were investigated using a new simple and quick HPLC-DAD method which allowed a very good resolution of all the analytes studied. The method was validated with respect to specificity, linearity, precision, accuracy and robustness. The structures of the main degradation products were investigated and confirmed by GC/MS technique.

3.1.1. *Materials and experimental procedures.*

a.   Chemicals and Samples

LND, ICA, DBC and IND were purchased from Sigma–Aldrich (Milan, Italy). IS was isolated as a secondary product from the alkylation of ICA with DBC to synthesize LND following the classical reaction of Silvestrini (Corsi et al., 1976). For this purpose, ICA was reacted with 3 equivalents of aqueous NaOH and 1 equivalent

of DBC, stirring the solution at 50°C for 7 h. The mixture solution was then fractionated on a silica column and the fractions were analyzed by HPLC. IS was isolated and its identity was confirmed by comparing the UV spectrum from DAD with that reported in literature and by GC/MS. The fraction was dried under high vacuum at 60°C for at least 48 h and IS was obtained as a white powder.

Phosphoric acid 85% p.a. was obtained from Sigma–Aldrich (Milan, Italy), methanol and water for HPLC from J.T. Baker (Holland). PTFE 0.45 μm membrane filters were purchased from Supelco (Milan, Italy). All other reagents were of the highest purity commercially available. The specialty Doridamine® tablets (30 mg) was commercially obtained.

Stock solutions of all the single compounds were prepared by dissolving appropriate amounts in methanol. The reference solutions were prepared by diluting with methanol the respective stock solutions to the final concentrations of LND (10.0–200.0 mg L^{-1}), ICA, DBC, IS, LDC, IND (0.5–50.0 mg L^{-1}) in volumetric flasks. A series of mixture solutions were prepared with all the analytes within the same concentration ranges of the single-component standards. The ratio between the impurities and LND was maintained in a percentage range from 1 to 83%. In all degraded samples the percentage of any impurity never exceeded the value of 83% with respect to starting LND. All solutions were stored in the refrigerator (4 °C) before analysis.

The content of five tablets of the specialty Doridamine® was pulverized and the equivalent to one tablet was suspended in methanol in a 25.0 ml volumetric flask. The suspension was sonicated for 10 min and then filtered through a 0.45 μm PTFE membrane. Samples for HPLC analysis were obtained by diluting 1 ml of the filtrate to 10.0 ml with methanol.

b.   Analytical instruments

HPLC analysis was carried out by using a HP 1100 pump fitted with a diode array detector G1315B (Agilent Technologies) and a Rheodyne 7725 manual injector. The LC column was a C18 Gemini (Phenomenex), 250 x 4.6 mm x 5 μm. The mobile phase consisted of methanol–phosphate buffer (pH 3) (80:20, v/v) at room temperature. The mobile phase was pumped isocratically at a flow rate of 1.5 ml min^{-1} during analysis. The injection volume was 5 μl. The optimum wavelength for the detection of all analytes with adequate sensitivity and specificity was found to be 275 nm. Gas-chromatographic (GC-MS) analysis was performed by a gas chromatograph Agilent 6890N with a Mass Selective Detector Agilent 5973. The GC conditions were as follows: column, HP capillary (30 m x 0.25 mm i.d.); 250 nm film thickness; injection port temperature, 250 °C; carrier gas, helium; flow-rate 0.3–0.6 ml min^{-1}; column temperature, programmed from 60 to 280 °C at 13 °C min^{-1}; initial time 3 min, final time 54 min.

Forced photodegradation was conducted in a light cabinet Suntest CPS+ (Heraeus, Milan, Italy), equipped with a xenon lamp. The apparatus was fitted with an electronic device for irradiation and temperature measuring and controlling inside the box. The system was able to select spectral regions by interposition of filters. In the present study, samples were irradiated under a direct lamp, with interposition of a single quartz filter, furnishing irradiation over 270 nm, and then between 320 and 800 nm, by means of a glass filter, according to the ID65 standard of ICH rules.

3.1.2.   Experimental results and discussion.

Several analytical columns were tested to achieve an optimal resolution of LND and the major related substances in its synthesis, shown above in figure 3.2. The Phenomenex Gemini C18 reversed-phase bonded phase provided the best peak

shape and sample resolution. This phase is designed for extended pH stability (pH range 1–12). Different mobile phases consisting of methanol and phosphate buffer were tested and the pH of the buffer was varied from 2 to 6 with 85% phosphoric acid. The best results were obtained using a mobile phase consisting of methanol and phosphate buffer in the ratio 80 : 20 (v/v), pH 3.0 in such a way as to achieve a
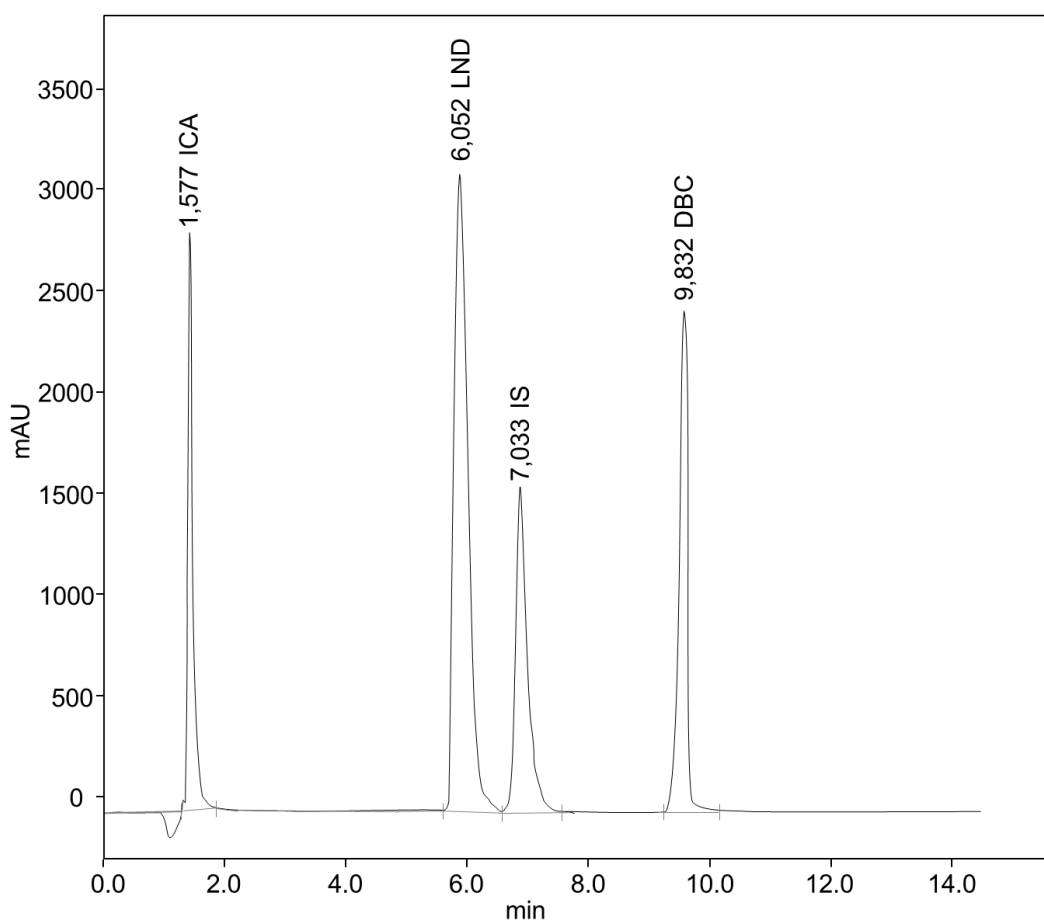
Figure 3.2 - Chromatogram of a standard mixture with Ionidamine and potential synthesis impurities: LND 100 mg L^{-1}, ICA, IS, DBC 50 mg L^{-1}

stable baseline and better peak shapes. The mobile phase was isocratically eluted with a flow rate of 1.5 ml min^{-1}. The analysis time was maintained less than 11 min in which all the components were well resolved. Under the described conditions, it is possible to observe a good separation between all the peaks, with LND eluting at

6.05 min. The reagent products ICA and DBC eluted at 1.58 and 9.83 min, respectively, whereas the isomer IS eluted at 7.03 min. These data confirm that the method developed can be suitable as a rapid and reliable quality control method of LND as a bulk material.

a. *Optimization and validation of chromatographic method.*

Chromatographic separation was optimized with respect to the stationary and mobile phase compositions, flow rate, sample volume and detection wavelengths. The method was opportunely validated to demonstrate suitability for routine application. The resolution of individual components and repeatability of injections were evaluated by retention time and peak area values. Calibration curves of LND and the other main products were calculated from data of 10 reference solutions of each compound, with concentrations ranging between 10 and 200 mg L^{-1} for LND and 0.5 and 50 mg L^{-1} for the impurities, distributed on 5 levels and analyzed in triplicate. The relative peak areas (dependent variables) were correlated to the respective drug concentrations (independent variables). The correlation coefficients were all higher than 0.98. The homoscedasticity of replicate measurements over the concentration ranges explored was tested to verify that the variances of measurements are independent of the concentration levels. The homoscedasticity was calculated by Cochran's test (Vetuschi et al., 1989) in which the parameter Cochran C (relative to n standards with p replicates) should be less than a critical value for each drug. The critical value for C5,3 at 95% confidence interval is 0.684. The six calibrations passed the homoscedasticity test since the C values were less than the critical value. The regression equations were validated by assaying an external set of 10 synthetic standard mixtures, with component concentration in the same range of the calibration set. The method showed percent recovery between

97.4–102.3 % and 95.7–103.5 % for the drug and for the impurities, respectively, and values of %RSD never above 3. The results of accuracy (%recovery) and precision (standard deviation) from application of HPLC analysis on this prediction set are listed in table 3.1. The study of interday and intraday precision at different concentration levels was performed by analysing several standards of known concentration. The method provided good precision for interday and intraday measures independent of the concentration, with a relative standard deviation (%RSD) between 1.9–4.2 % and 2.4–5.8 %, respectively. Thus, the repeatability and reproducibility of the method were satisfactory. The robustness of the HPLC method was determined by observing the influence of limited changes in the mobile-phase composition on the peak areas and retention times. Where the changes were maintained under a value of ±6 %, relative peak areas related to the peak areas for optimal mobile phase composition resulted in a range from 95 % to 105 %. When the change exceeded the value of ±6 %, some peaks were not completely separated. The next study was a stability study, carried out by exposing LND in both solid and solution forms under stressing conditions. Degradation of the drug was examined under heat and light exposure.

Table 3.1 - Accuracy (% recovery) and precision results (Standard Deviation) from application of HPLC analysis on the prediction set. The nominal values are expressed as mg L^{-1}.

Sample	Nominal						Found					
	LND	ICA	DBC	IS	IND	LDC	LND	ICA	DBC	IS	IND	LDC
1	10.02	0.52	1.83	4.50	14.85	50.22	98.20	94.91	102.28	94.91	94.76	95.48
2	25.05	1.56	5.49	13.50	44.55	0.62	87.70	103.24	101.74	96.27	99.07	100.21
3	50.1	4.68	16.47	40.50	0.55	1.86	99.40	95.67	100.42	98.31	98.24	98.41
4	100.2	14.04	49.41	0.50	1.65	5.58	102.10	94.07	98.07	100.22	103.33	99.27
5	200.4	42.12	0.61	1.50	4.95	16.74	100.98	95.29	99.50	101.48	98.37	102.74
6	10.02	4.68	49.41	1.50	14.85	0.62	99.02	94.75	96.29	103.2	99.21	101.78
7	25.05	14.04	0.61	4.50	44.55	1.86	102.30	102.53	94.80	102.21	101.04	103.11
8	50.1	42.12	1.83	13.50	0.55	5.58	97.40	101.21	101.90	100.74	97.70	98.24
9	100.2	0.52	5.49	40.50	1.65	16.74	101.50	100.98	95.03	97.28	100.21	97.72
10	200.4	1.56	16.47	0.50	4.95	50.22	100.08	99.27	96.24	99.44	94.88	95.29

Mean	*98.87*	*98.17*	*98.63*	*99.41*	*98.64*	*99.23*
SD	*1.74*	*2.23*	*2.01*	*2.98*	*2.56*	*2.43*

b.   Thermal degradation

Two series of six LND methanol solutions 100 mg l^{-1} in sealed vials were maintained in a thermostatic oven at 40 and 60 °C, respectively. HPLC analysis was run just after sample preparation (t = 0) and at the following times: 2, 5, 10, 20, 30 days. Thermal degradation tests were also performed on the solid product, kept in sealed vials and maintained in a thermostatic oven, at 60 and 100 °C. HPLC analysis was run at t = 0 and at the following times: 10, 20, 60, 90 days. Analogous samples of LND, in solution and in solid state, were maintained at 21 °C and analyzed at the same times. The sample maintained at 40 °C showed no significant changes along the entire test, demonstrating very high stability. In contrast, the sample kept at 70 °C showed the formation of a new peak at 13.85 min and the simultaneous decrease of the LND peak. This degradation product was identified by GC/MS analysis as the decarboxylated form of LND (LDC), with a molecular signal with m/z 277 and the characteristic signals m/z 118, corresponding to the indazole derivative, and m/z 162 corresponding to the indazole carboxylic derivative. A series of secondary products were detected in small amounts with retention times under 6 min but their identification was not carried out. After 30 days the residue percentage of LND resulted to be 37 %. A HPLC chromatogram of a thermally stressed LND sample under 70 °C is shown in figure 3.3.
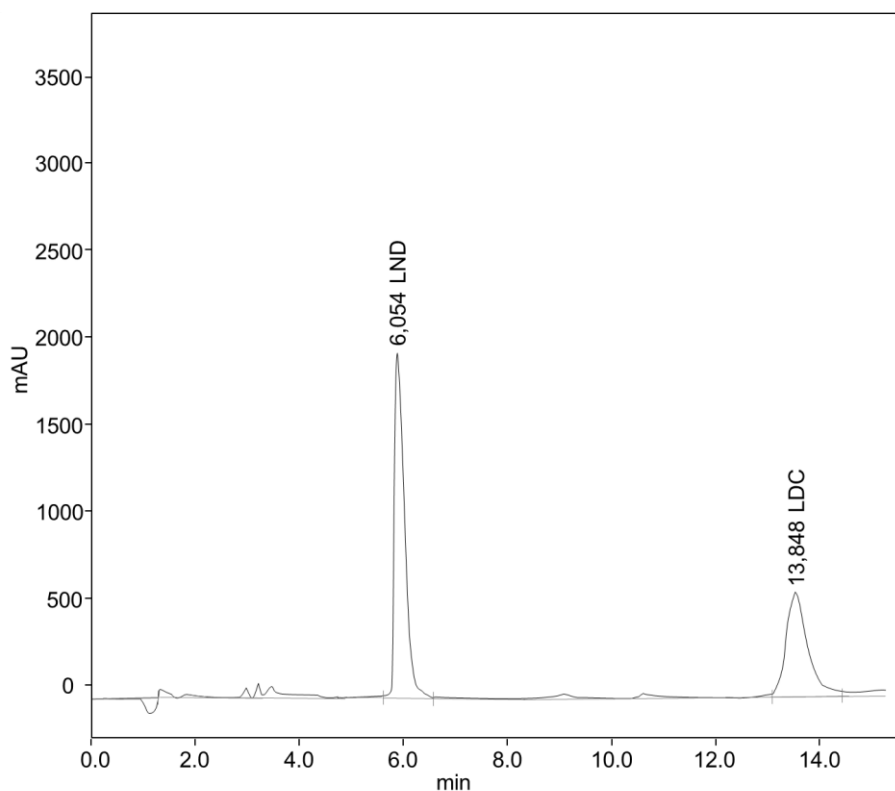
Figure 3.3 - HPLC chromatogram of a 100 mg L^{-1} LND solution
kept at 70 °C for 30 days.

For the control, standard solutions of LND in methanol at the same concentrations were kept at room temperature (25 °C) and in a refrigerator (4 °C). No significant changes in the content of LND were observed during the storage at both conditions even after 90 days. The thermal stressing tests were also performed on the solid product, kept in closed vials at 60 and 100 °C and analyzed every 10 days up to a final time of 90 days. Only traces of LDC occurred in these experiments, confirming the high stability of solid LND under stressing temperature.

c. Photodegradation

In the present study, samples were submitted to forced photodegradation in the light cabinet Suntest CPS+ under two different conditions. In a first test series, six samples of LND 100 mg L^{-1}, were subjected to direct irradiation of the xenon lamp

27

with interposition of only a quartz filter, corresponding to a wavelength range between 270 and 800 nm. In a second test series, six LND solutions with the same concentration were irradiated under a wavelength range between 320 and 800 nm, by means of glass filters, according to the ID65 standard of ICH rules. In both the experiments, the irradiation power was fixed at 350 W m^{-2}, corresponding to an energy value of 21 kJ (min m^2)$^{-1}$. The inner temperature was maintained constant at 25 °C in all these experiments. HPLC analysis was run just after sample preparation (t = 0) and at the following times: 5, 15, 30, 60, 90, 120, 150, 210, 270, 330, 390, 450, 510, 600 min. Photodegradation tests were also performed on the solid product, kept in sealed vials, under the above described conditions. HPLC analysis was run at t = 0 and at the following times: 5, 10, 30, 60, 90 h. Samples of ICA 50.4 mg ml^{-1} and IND 50.5 mg L^{-1} were also submitted to forced irradiation for studying the photodegradation mechanism of LND. When the first experiment with irradiation over 270 nm was performed, a first photoproduct appeared after 30 min with a retention time of 1.58 min. This product was identified to be ICA, derived from the debenzylation of LND. Its concentration increased constantly during degradation up to a value of 12.4 mg L^{-1} after 600 min, calculated by means of the regression equation. When the logarithmic values of the concentration percentage (LND%) were plotted against the degradation time (min) up to 120 min, a straight line was obtained, according to the following equation:

1)   Log LND% = 0.001 t + 1.9997

where 0.001 is the photodegradation rate constant, t the time (min) and 1.9997 is the experimental logarithmic value of the starting concentration percentage (100%). After about 120 min, the forced irradiation induced a more complex

28

degradation, with the appearance of a peak at 13.85 min, identified as LDC, the decarboxylated by product of LND. Its content reached the value of 13.5 mg L^{-1} after 600 min, calculated by the relative equation. At the same time, the simultaneous formation of other two main photoproducts presenting signals at 5.26 (PP1) and 9.01 (PP2) min was revealed, both increasing all through the experiment. Simultaneously, a number of other secondary products were formed but their contents remained low or at trace levels. Unfortunately, isolation of these products was very hard and their characterization was not carried out. The gradual disappearance of LND was recorded up to a residue value of about 12 mg L^{-1}. In figure 3.4 the HPLC chromatogram of a LND sample after 210 min of forced irradiation is shown.

In order to identify the two photoproducts PP1 and PP2, degradation experiments were also performed on the products ICA and IND, assuming that they can be secondary photoproducts after decarboxylation and debenzylation of LND. IND samples showed a remarkable stability and after 240 min the percentage of residual product was found to be 97 % with the formation of some degradation products, but all in low or trace amounts, and none of them coincided with the products investigated.
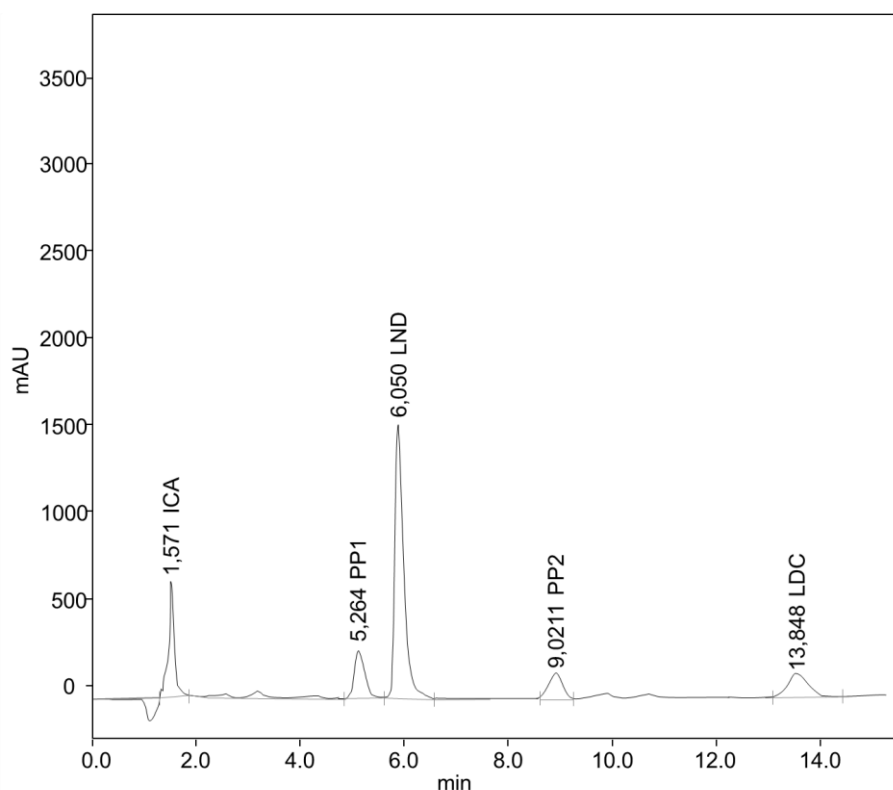
Figure 3.4 - HPLC chromatogram of a 100 mg L^{-1} LND solution kept under stressing irradiation for 210 min.

In contrast, degradation of ICA showed the formation of several degradants including two of them with retention times close to those of PP1 and PP2 and similar spectroscopic characteristics. In fact, the DAD signals of both these degradants presented UV spectra with a clear decrease of the absorbance in the zone 275–325 nm. This absorbance signal is present in the spectra of all the main products in the present study, including LND, ICA, IND, IS and LDC. The unknown degradants from LND irradiation were so hypothesized to be secondary products from degradation of ICA, in turn derived from debenzylation of LND.

The second degradation experiments, in which the LND samples were treated under irradiation between 320 and 800 nm, showed a lower degradation compared to that previously reported, with a LND residual concentration of 90 % after 600 min

of irradiation. The mean photoproduct formed in these experiments was ICA, reaching a concentration of about 5.1 mg L^{-1}. Only traces of LDC and of the same photoproducts PP1 and PP2 described in the previous experiment were revealed.

These results demonstrated that LND is sensitive to light, but its degradation is significant only in the presence of high energy light, with wavelengths shorter than 320 nm. In normal conditions of manufacturing or storage of the drug, when the product is protected from the so-called window-filter, the product is quite stable. The adoption of suitable measures in the processing and packaging of the drug can certainly be effective in protecting the drug from light degradation and minimizing degradation at insignificant levels. A scheme of the hypothesized degradation of LND under stressing thermal and irradiation conditions is summarized in figure 3.5.
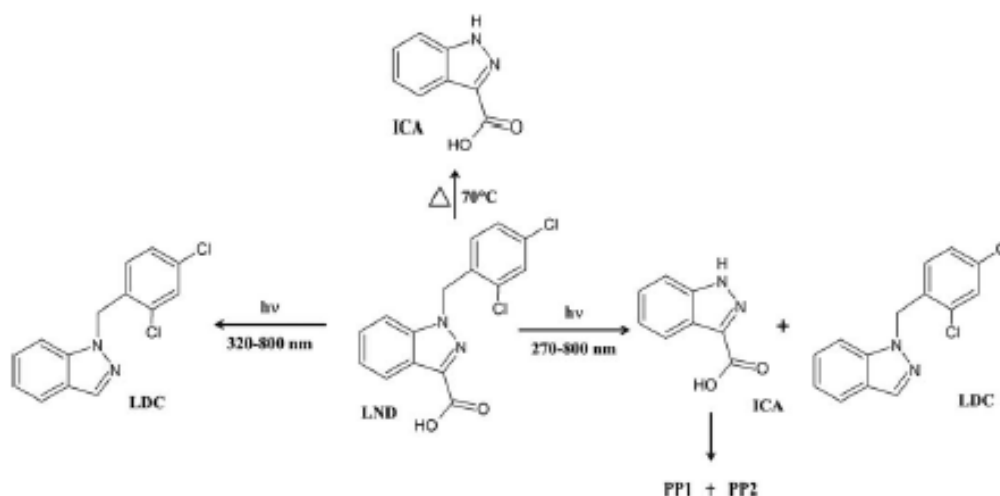

Figure 3.5 - Proposed degradation of LND under stressing thermal and irradiation conditions

d.   Real samples

Both thermal and photodegradation tests were directly performed on real samples of tablets from three different Doridamine® packages (LND 30 mg) and on the tablets in the original first packaging. For each package, six tablets were exposed

to 40 and 70 °C, respectively, and analyzed by HPLC at 2, 5, 10, 20, 30 days. The samples showed no significant change after an exposure time of 10 days; after that traces of the decarboxylated product LDC, under the LOD value, were detected.

Six tablets for each experiment were treated with forced irradiation in the light cabinet under both the conditions reported above and analyzed by HPLC at 60, 120, 240, 480 and 960 min. When irradiation between 320 and 800 nm was adopted, only traces of ICA were detected but the content of LND did not show significant decrease. Under the stressing irradiation with wavelengths below 320 nm, the peaks of the degradants LDC and ICA were revealed in traces after 240 min but their content did not increase significantly up to 960 min. The content of LND did not change significantly along the entire test. The photodegradation tests on the tablets in their packaging showed in all the tests a complete stability of the formulation.

3.2. Study on photodegradation kinetics of melatonin by multivariate curve resolution (MCR) with estimation of feasible band boundaries.

Spectrophotometric methods are widely used in the determination of several analytes and for the investigation of many analytical problems (Skoog and West, 2004). However, traditional spectrophotometric methods, using a few number of wavelengths, are often not sufficient to provide the sought information to solve a multicomponent system, especially when the spectra are highly overlapped. In recent years, different multivariate approaches have been proposed to extract useful information from UV data (Massart et al., 1998). Multivariate methods have the advantage of exploiting all the information, simultaneously using a very large number of analytical signals.

Multivariate Curve Resolution - Alternating Least Squares (MCR-ALS) is one of the recent chemometric techniques frequently used for the analysis of spectrophotometric data (Javidnia et al., 2008; de Juan et al., 2000). It is able to resolve the different sources of variance in a particular data set and it allows the study of complex evolving chemical processes, estimating the number of components, their pure spectra and concentration profiles. When the investigated process is a kinetic reaction, it allows also the estimation of rate constants (*k)* (De Luca et al., 2010). MCR-ALS, like Principal Component Analysis (PCA) (Brown et al., 2009), performs a bilinear decomposition of the experimental data matrix in the product of two factor matrices of reduced size. This mathematical decomposition is performed under constraints with more physical meaning and easier interpretation than in PCA bilinear decomposition, in which the orthogonal type of constraints are used (Tauler, 2007). However, the solutions obtained by MCR methods are often not unique because of the intrinsic rotational and intensity ambiguities (Tauler et al.,

1995) and a set of feasible solutions that fit equally well the experimental data can be obtained instead. This extent of rotation ambiguity can be drastically reduced or eliminate depending on the applied constraints and on the intrinsic data structure. Non negativity, closure, unimodality, selectivity and local rank constraints are usually applied (de Juan et al., 1997; Gargallo et al., 1995) to improve MCR solutions.

MCR-ALS methods have been already applied to UV spectrophotometric data for the interpretation of kinetics of drug photodegradation (De Luca et al., 2010; Mas et al., 2008). In these previous works, MCR-ALS methods have been used for the elucidation of photodegradation kinetic processes, allowing at the same time the estimation of the spectra of photoproducts and intermediates.

Photostability of drugs represents an important issue in pharmaceutical research and a very large number of compounds have been described to be photolabile (Cornelissen and Beijersbergen van Henegouwen, 1979; Tønnesen, 2001; Albini et al., 1997; Beijersbergen van Henegouwen, 1997). A deep knowledge of the drug photo-reactivity is effectively essential for a correct pharmaceutical formulation and its packaging. A standard protocol for photostability drug testing is described in ICH Guidelines, which constitute the recommended set of procedures in pharmaceutical industry for key testing of new drugs (ICH; 1996).

Melatonin (N-acetyl-5-methoxytryptamine) (ML) is a neurohormone produced mainly by the vertebrate pineal gland and synthesized from L-tryptophan (Pandi-Perumal et al., 2008; Axelrod and Wurtma, 1968). It is an important component of the body's internal time keeping system and is involved in important physiological events, such as the circadian rhythms (sleep-wake cycle). Alterations in ML metabolism have been demonstrated in circadian rhythm sleep disorders, Alzheimer's and Parkinson's diseases, glaucoma, depressive disorders, breast and prostate cancer, hepatoma and melanoma (Dahlitz et al., 1991; Brugger et al., 1995). In pharmaceutical therapy,

ML is used to balance possible metabolic disorders or regulate circadian rhythm, sleep disorders, insomnia in blind people, intercontinental flight dysrhythmia (jet-lag syndrome) and insomnia in elderly patients (Leger et al., 2004).

ML is known as a photolabile drug and its exposure to light causes a deep transformation of its chemical structure with a probable loss of therapeutic activity. The phodegradation process (Fig. 3.6), described in previous publications (Andrisano et al., 2000), consists in the oxidation of the indole ring to give the N-{3-[2-(formylamino)-5-methoxyphenyl]-3-oxopropyl}acetamide (MLD) through an endoperoxide intermediate.
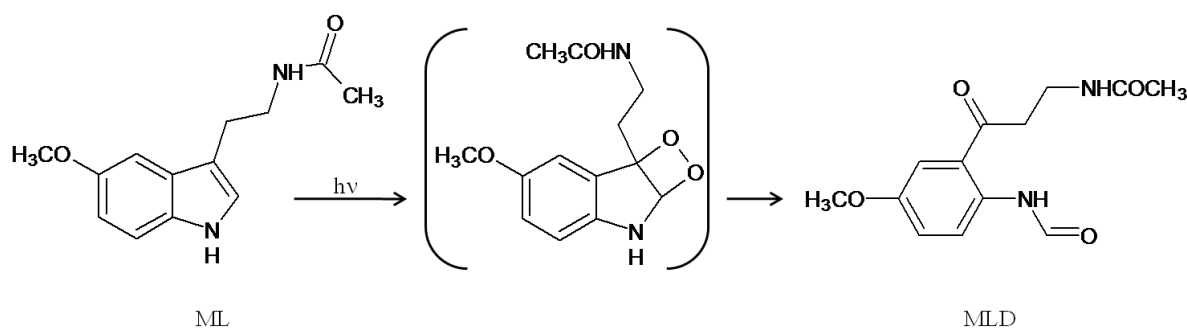
Figure 3.6 - Hypothesis of photodegradation mechanism of ML giving MLD

In our previous application note (De Luca and Ragno, 2009), the kinetic pathway involved in the photodegradation process of ML was resolved by MCR-ALS. However, these results suffered of a moderate uncertainty in estimating both the spectra of the degradation products and the rate constants of the reaction. In this work, the photodegradation mechanism of ML was investigated more thoroughly by applying MCR-ALS on spectrophotometric data. In particular, rotational and scale ambiguities affecting MCR results were studied in detail using a procedure proposed

by Gemperline for the calculation of their extent under a set of constraints (Gemperline, 1999). In particular, a non-linear curve fitting routine (Hard/Soft-MCR-ALS) was used to constrain the MCR-ALS solutions to follow the proposed kinetic reaction model and reduce the extent of rotational ambiguities. Thus unique solutions and rate constants were obtained. The study allowed elucidation of the dependence of the kinetic rates of ML degradation on different values of light irradiation power.

3.2.1   Materials and experimental procedures.

a.   Chemicals and instruments

ML was purchased from Sigma-Aldrich Co. (Italy). Spectrophotometric grade ethanol was from J.T. Baker (Holland).

Light exposure was performed in a light cabinet Suntest CPS+ (Heraeus, Milan, Italy), equipped with a Xenon lamp. The apparatus was fitted up with an electronic device for light irradiation and temperature measuring and controlling. The system was able to closely simulate sunlight and to select spectral regions by interposition of appropriate filters.

Spectrophotometric measurements were recorded using an Agilent 8453 Diode Array spectrophotometer (Agilent Technologies. USA).

All chemometric analyses were performed under MATLAB computer environment (The Mathworks Inc., MA, USA). MCR-ALS (both command line and GUI versions), HS-MCR-ALS (only command-line version) and MCR-BANDS (both command line and GUI versions) computer methods were implemented as MATLAB functions. They have been used as described in previous works (de Juan et al., 2000). Source files containing these algorithms are available under request to one of the authors of this work or visiting the web site "www.mcrals.info". MCR-BANDS additionally

requires the use of *fminuncon, fminsearch* and *fmincon* functions from the version 3 or higher of the MATLAB Optimization Toolbox.

b.   Experimental procedures

All photodegradation experiments were performed following the ICH recommendations for drug stability tests.

Stock solutions of ML (1 g L^{-1}) in ethanol were properly diluted to obtain the samples (20 mg L^{-1}) for degradation experiments. These samples, in quartz cells perfectly stoppered, were directly light irradiated according to the ID65 standard of the ICH rules. The wavelength range was set between 300 and 800 nm, by means of a glass filter, and the irradiation power was changed at four different levels: 250, 350, 450 and 550 W m^{-2}, corresponding to energy values of 15, 21, 27 and 33 kJ (min m^2)$^{-1}$, respectively. The inner temperature was maintained constant at 25 °C in all these experiments.

UV spectra were recorded in the wavelength range of 200-450 nm, just after sample preparation (t = 0) and at the following times: 20, 40, 60, 80, 100, 120, 140, 160, 180, 200, 220, 240, 260, 280, 300, 320, 340 and 360 min.

3.2.2.   Chemometric techniques

a.   Evaluation of the extent of rotation ambiguities using the MCR-BANDS procedure.

As mentioned chapter 2, MCR-ALS solutions, under a particular set of constraints, can still be not unique because of the presence of unsolved rotational ambiguities. In this case, instead of getting a unique solution, a set of feasible solutions that fit equally well the data matrix **D** can be obtained. In the literature, this

problem has been reported as factor analysis ambiguity (Tauler et al, 1995; Tauler et al, 1993). Rotational and intensity ambiguities can be represented through equation:

$$1) \qquad \mathbf{D} = \mathbf{C}_{old}\mathbf{S}_{old}{}^T = (\mathbf{C}_{old}\mathbf{T})(\mathbf{T}^{-1}\,\mathbf{S}_{old}{}^T) = (\mathbf{C}_{new}\mathbf{S}_{new}{}^T)$$

For any non-singular matrix **T** (**T** should be invertible), a new set of solutions is obtained which describes equally well the data matrix **D**. The number of feasible solutions and possible **T** values (new **C** and **S**^{T} matrices) can be drastically reduced by applying constraints derived from the physical nature and previous knowledge of the studied system. In our case, as it was previously mentioned, non-negativity (concentrations and spectra of the components must be positive), unimodality (concentration profiles throughout the degradation process present only one maximum per experiment) and closure (mass balance in the kinetic process) constraints were adopted (de Juan et al., 1997; Gargallo et al., 1995; R. Tauler et al., 1995). In some favourable cases, it is also possible to perform an improved resolution of the system using other constraints related to selectivity in concentration or spectral regions[8] or related to the knowledge of local rank conditions (Manne, 1997) if they are present.

For each species profile, the set of feasible solutions under constraints defines a range or band of feasible solutions, and this band may be delimited by maximum and minimum band boundaries estimated using a particular criterion. These boundaries will be related to specific rotation matrices **T** for each species k, which will be called $\mathbf{T}_{max,k}$ and $\mathbf{T}_{min,k}$. By considering a particular pair of solutions to Equation 1, $\mathbf{C}_{inic}$ and $\mathbf{S}_{inic}{}^T$, the maximum band boundaries, $\mathbf{C}_{max,k}$ and $\mathbf{S}_{max,k}{}^T$, and the minimum band

boundaries, $\mathbf{C}_{min,k}$ and $\mathbf{S}_{min,k}^T$, may be defined, respectively, by the following equation:

2)　　$\mathbf{D} = \mathbf{C}_{inic}\mathbf{S}_{inic}^T = \mathbf{C}_{inic}\mathbf{T}_{min,k}\mathbf{T}_{min,k}^{-1}\mathbf{S}_{inic}^T = \mathbf{C}_{min,k}\mathbf{S}_{min,k}^T = \mathbf{C}_{inic}\mathbf{T}_{max,k}\mathbf{T}_{max,k}^{-1}\mathbf{S}_{inic}^T = \mathbf{C}_{max,k}\mathbf{S}_{max,k}^T$

Different procedures to define the band boundaries have been reported (Tauler, 2001; Kim and Henry, 1999; Henry and Kim, 1990). In this work, the optimization algorithm for the calculation of the band boundaries of feasible solutions was based on a non-linear constrained optimization of an objective function defined by the ratio between the signal contribution of a particular species and the whole measured signal (Signal Contribution Function, *SCF*) (Gemperline, 1999). It is calculated by the equation:

3)　　$SCF_k = \dfrac{\left\| \mathbf{c}_k \mathbf{s}_k^T \right\|}{\left\| \mathbf{CS}^T \right\|}$

where SCF_k is a scalar value which gives the relative signal contribution of a particular component to the whole signal for the mixture of N components (k=1,…N). This relative signal contribution function, SCF_k, is measured as the quotient between two norms (Frobenious norm), the first one from the signal of the considered component k, $\|\mathbf{c}_k\mathbf{s}_k^T\|$, and the other from the whole signal considering all the components, $\|\mathbf{CS}^T\|$. The product $\mathbf{CS}^T$ is constant, as fixed in Equation 7, and it remains constant for any invertible matrix $\mathbf{T}$. On the contrary, every $\mathbf{T}$ matrix gives a different set of $\mathbf{c}_k$ and $\mathbf{s}_k^T$, so their product $c_k s_k^T$ will be also different, as well as its

norm $\|\mathbf{c}_k\mathbf{s}_k^T\|$ and SCF_k defined in equation 9. Therefore, the SCF_k is a scalar value, which will depend on the considered **T** matrix, which will depend on a particular set of constraints. The goal of the procedure is to find the **T** matrices ($\mathbf{T}_{max,k}$ and $\mathbf{T}_{min,k}$) that give the maximum and minimum SCF_k values ($SCF_{max,k}$ and $SCF_{min,k}$) for every k component involved in a system **C** and $\mathbf{S}^T$ (Tauler, 2001).

The profiles giving these maximum and minimum band boundaries were calculated using the MCR-ALS solutions obtained in the analysis of the augmented matrix obtained from the photodegradation experiments of ML samples at every irradiance power condition.

b.   Hybrid hard- and soft-multivariate curve resolution (HS-MCR)

A new constraint can be introduced during the ALS optimization to force the concentration profiles in matrix **C** to fit a previously selected kinetic model. This procedure, which has been named as hard–soft multivariate curve resolution-alternating least squares (HS-MCR-ALS) modelling, applies a hard modelling constraint based on an additional non-linear kinetic curve fitting routine during each ALS iteration, which forces concentration profiles in matrix **C** to fulfil a preselected kinetic model with their corresponding rate constants (Maeder and Zuberbuhler, 1990) adjusted during the ALS procedure. The resulting concentration profiles will fit the proposed kinetic model and the corresponding rate constants of the process will be obtained as additional valuable information.

Furthermore, HS-MCR-ALS permits the simultaneous analysis of multiple data matrices obtained under different conditions and having different kinetic reaction models and rate constant values, in such a way to optimally resolve the experimental

augmented data matrix $\mathbf{D}_{aug}$ (see equation 6) from different photodegradation experiments.

In this work, the ML photodegradation mechanism was adequately described by a first order kinetic model, with a rate constant dependent on the irradiance power of the light source used during the degradation experiments.

3.2.3. Experimental results and discussion

a. MCR analysis of the photodegradation experiments

Figure 3.7 shows the spectral sequences of the photodegradation experiments. Spectra from four ML sample solutions (20 mg L^{-1}) under different conditions of light irradiance were recorded during 360 min. Light power was set at 250, 350, 450 and 550 W m^{-2}, respectively. The differences observed in figure 3.7 confirmed a significant increase in the photodegradation rate when the irradiation power increased.
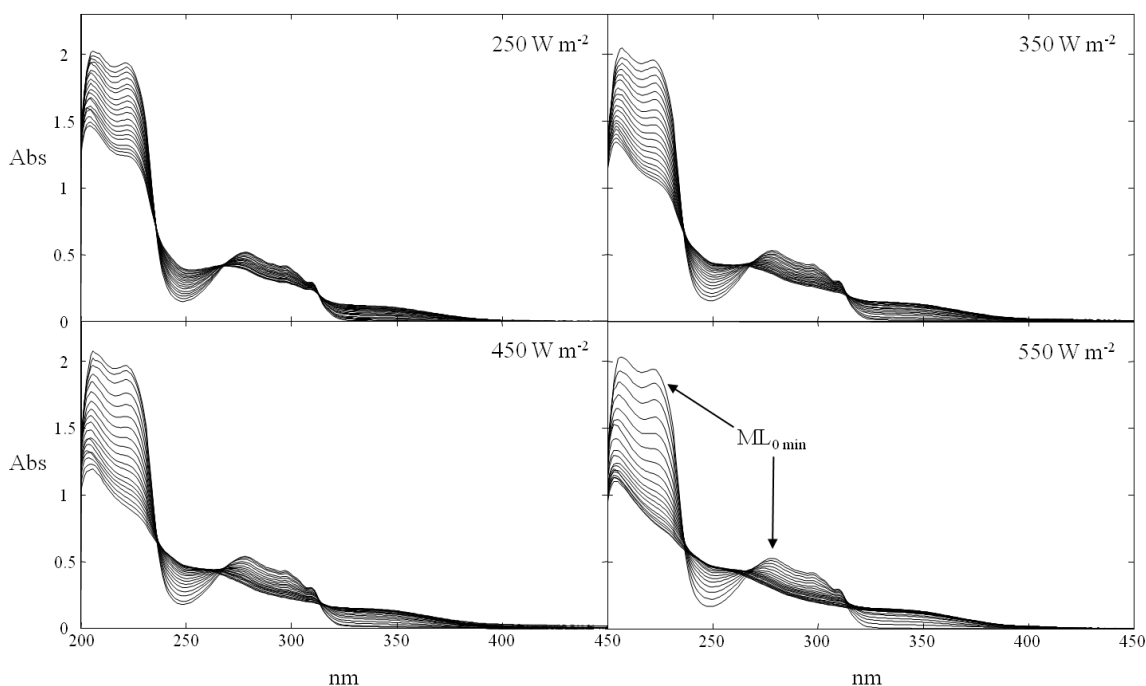

Figure 3.7 - UV-spectra of photodegradation experiments of ML (20.0 mg L^{-1}), exposed under light at 250, 350, 450 and 550 W m^{-2}

Rank analysis (SVD) of the augmented column-wise data set, $\mathbf{D}_{aug}$ in equation 1, consisting of the data from the four degradation processes, showed the presence of two different species. Initial estimations of the pure spectra of these two species were already obtained using the purest variable detection method. These spectra were identified to correspond very closely to the known pure spectra of ML and MLD. It was not possible to detect by ordinary UV absorption spectroscopy the peroxide intermediate, probably due to its extremely short life. The spectral data set of figure 3.7 were analyzed using the MCR-ALS column-wise matrix augmentation procedure, applying non-negativity (both concentrations and spectra), unimodality (only concentrations) and closure (only concentrations) constraints. Values of *%lof* and *%R^2* resulted to be 1.53% and 99.96%, respectively.

The shapes of the pure species concentration profiles were in agreement with a first order reaction kinetic model (ML→MLD).

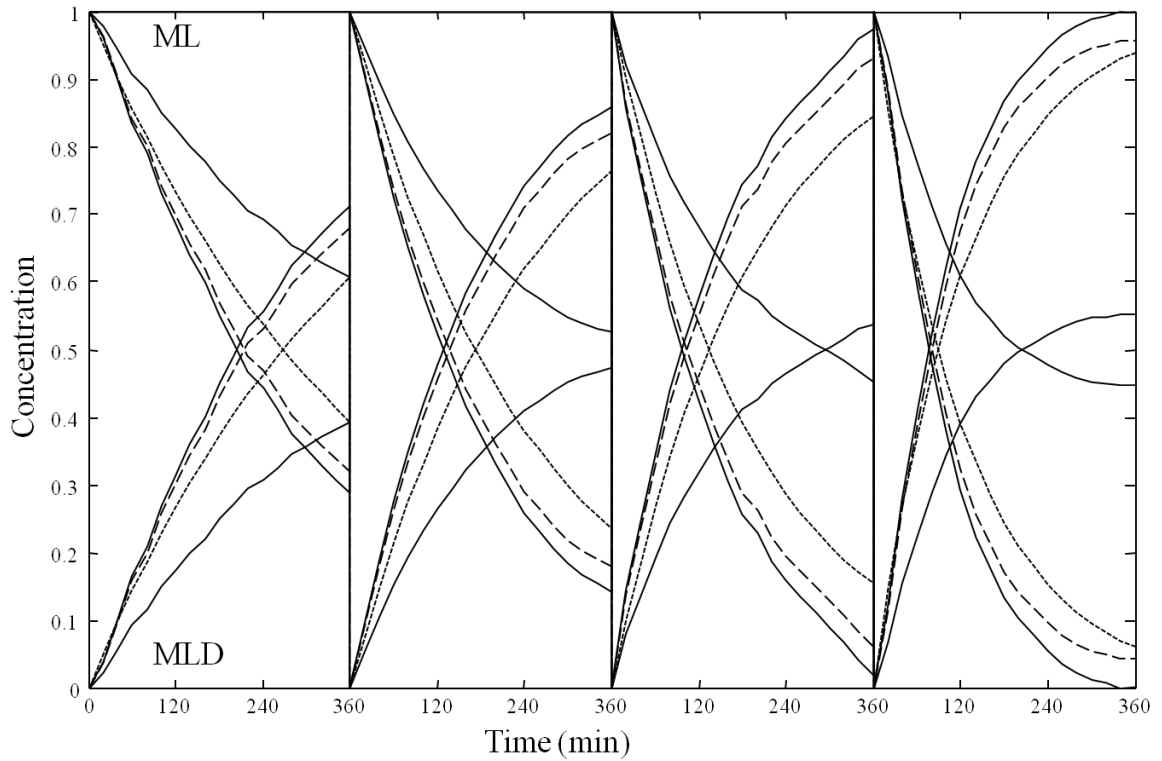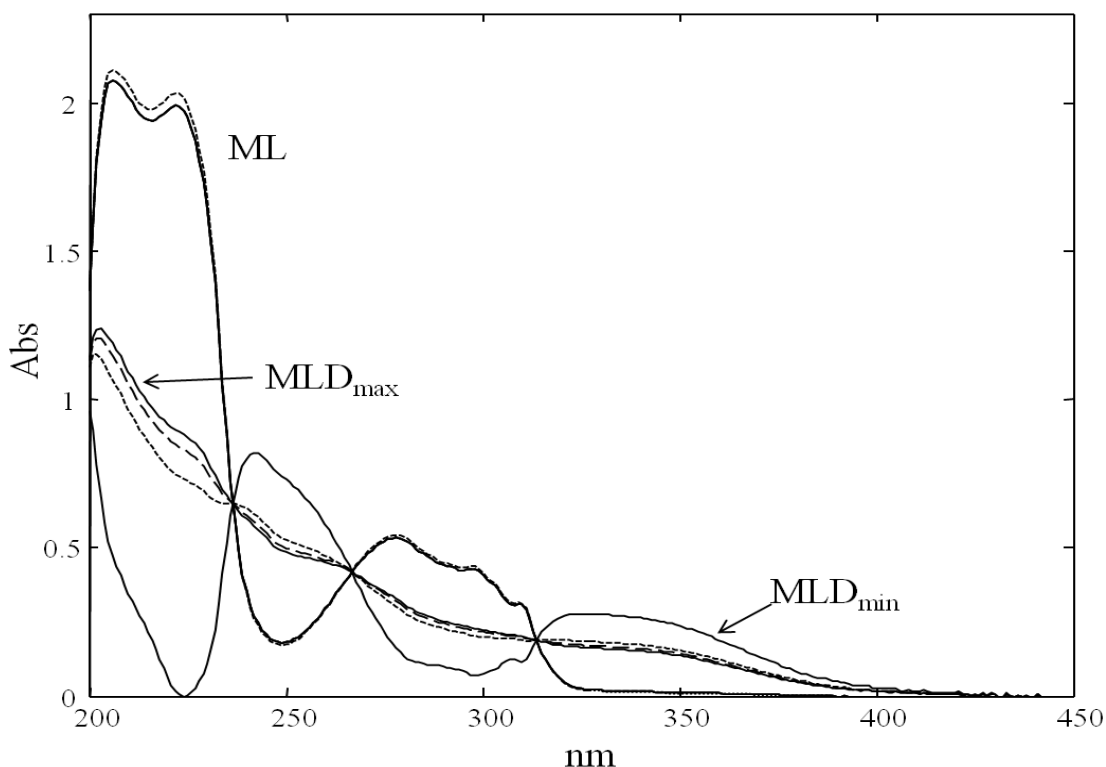*b.   Calculation of the extent of rotation ambiguities and of the boundaries of feasible solutions*

Figure 3.8 - Concentration profiles obtained from the simultaneous analysis of the four photo-degradation experiments of ML solution (20.0 mg L^{-1}): full lines are the band boundaries obtained by MCR-BANDS, broken lines are the profiles obtained using MCR-ALS, dotted lines are the profiles calculated by HS-MCR-ALS

Figure 3.9 - Spectra profiles obtained from simultaneous analysis of the four photo-degradation experiments of ML solution (20.0 mg L^{-1}): full lines are the band boundaries obtained by the MCR-BANDS procedure, broken lines are the profiles obtained using MCR-ALS, dotted lines are the true profiles calculated by HS-MCR-ALS, which are coincident with the known (normalized) pure spectra profiles of ML and MLD

Figures 3.8 and 3.9 show the extent of rotation ambiguities associated to concentration and spectra profiles obtained using MCR-ALS (broken lines) as initial estimates (C_{inic} and S_{inic}^T in equation 2). The band boundaries (continuous lines) were obtained using the non-linear optimization MCR-BANDS procedure, previously described in the method section. The dotted lines are the profiles obtained by the HS-MCR-ALS procedure. All these plots were obtained considering the simultaneous analysis of the four kinetic experiments and they show clearly that although the system was relatively simple (only two components), the extent of rotation ambiguities can still be relatively large. Band boundaries of Figures 3.8 and 3.9 describe the extent of rotation ambiguities and the set of possible solutions that fit

the data equally well and fulfil the imposed constraints: non-negative spectra and concentration profiles, unimodal concentration profiles and closed concentration profiles. For both species in the four experiments, one of the band boundaries is very close or coincides to the MCR-ALS solution, ML concentration profile is close to the minimum band boundary profile, while MLD concentration profile is close to the maximum band boundary profile. In particular, the concentration profiles of both species exactly coincide with the band at beginning of the experiments, where the rotational ambiguity of the MCR-ALS solution is absent. This is due to the favourable local rank conditions at starting of degradation, when only ML is present. Moreover, the effect of the favourable local rank conditions is also clear in the band boundaries of the spectra profiles, where the ML maximum and minimum band boundaries are practically identical to the MCR-ALS solution and the rotational ambiguity is only present for MLD), which has maximum and minimum band boundary profiles very different.

In order to reduce the extent of rotation ambiguities and assure the recovery of the true spectra and concentration profiles, the HS-MCR-ALS procedure was then applied to fit the particular reaction kinetic model. Kinetics ($\mathbf{C}$) and pure spectra ($\mathbf{S}^{\mathrm{T}}$) profiles obtained by HS-MCR-ALS analysis (broken lines) are also plotted in figures 3.8 and 3.9. These graphs confirmed that the HS-MCR-ALS solution is the one that recovers more perfectly the known spectra profiles (normalized) of ML and MLD. Therefore, by using the HS-MCR-ALS procedure, the ambiguity of the resolved solutions was practically totally removed. This confirms that HS-MCR-ALS eliminates rotation ambiguities associated to the application of MCR-ALS under soft constraints (like non-negativity, unimodality and closure) in the study of kinetic chemical reactions.

Table 3.2 - Kinetic constants for ML photodegradation under different conditions of irradiance power

Power (W m^{-2})	Kinetic constants
250	3.185E-03 $\pm$ 2.121E-05
350	4.351E-03 $\pm$ 2.859E-05
450	6.460E-03 $\pm$ 6.828E-05
550	1.008E-02 $\pm$ 6.737E-05

Table 3.2 lists the values of the rate constants of the ML photodegradation for every experiment. The percentage values of *lof* and *R^2* resulted to be 2.13% and 99.94%, respectively. The results from augmented MCR analysis pointed out a significant dependence of the photodegradation kinetics by the irradiation power. The rate constants of the postulated reaction were increasing with the increase of the light power, following an exponential tendency in according with the equation:

4) $\mathbf{y} = 0.0012e^{0.0039\mathbf{x}}$ ($R^2 = 0.994$)

where *y* is the k value and *x* the illuminance power (Wm^{-2}).

The reaction rate of photodegradation of drugs in solution has been reported to increase with the decrease of the drug concentration and with the increase of the illuminance power (Tao et al., 2005; Allowood and Plane, 1986). These results could be interpreted with a dependence of the photodegradation rate from the number of incident quanta of energy. This number is scarce when the illuminance power is low and therefore the photodegradation rate is limited. On the contrary, the number of

incident quanta is abundant when the illuminance power is high, so the rate tends to increase.

3.3. Study of pH-dependent photodegradation of amiloride by a multivariate curve resolution approach on combined kinetic and acid-base titration UV data.

Amiloride (3,5-diamino-N-(diaminomethylene)-6-chloropyrazine-carboxamide monohydro-chloride) (AML) is a diuretic agent widely used in therapy, alone or in formulations with drugs belonging to the same pharmaceutical class (Vidt, 1981). AML is known to be a photosensitive drug and its degradation causes worsening in patients, observed as an exaggerated sunburn (Magnus, 1977). AML photodegradation has been already studied and the influence of pH on the degradation process investigated (Calza et al., 2008; Li et al., 1999). Nevertheless, these studies have been performed by using traditional spectroscopic or chromatographic analysis, without taking into account the acid-base equilibrium of AML (pKa = 8.7). Really, the photodegradation process of AML resulted to be rather complex and involving many different photoproducts. AML is basic and, when its photodegradation takes place in water, simultaneous protonation can occur, depending on pH, and thus more chemical species could be subdued to light degradation and more photoproducts obtained (Lev and Veinberg, 2004).

In the last years, the study of multicomponent systems involving equilibria and kinetic chemical processes, such as the AML system, has been investigated by combination of spectrophotometry and chemometric methodologies with satisfactory results. Multivariate (multi-wavelength) spectrophotometric methods allow the analysis of a multicomponent system without any previous separation. Multivariate Curve Resolution - Alternating Least Squares (MCR-ALS) is one of the current chemometric techniques used for the analysis of spectrophotometric data (de Juan et al., 2000). MCR analysis, in its soft-modelling approach, does not require any

previous knowledge or model about the studied process and offers a fast and powerful tool for the mathematical resolution of unknown mixtures where the initial knowledge of the system is only partial or non-existent (de Juan et al., 2009; Rajko and Istvan, 2005; Gemperline, 1999; Wentzell et al., 1998). MCR methods are appropriate to describe the kinetics of drug photodegradation, allowing estimation of the pure spectra and concentration (time) profiles of the photoproducts (De Luca et al., 2011; De Luca et al., 2010; Mas et al., 2008). However, this approach can have some limitations in estimating the number of species involved in the process and in their proper resolution (Golub and Reinsch, 1970). This phenomenon is known in the literature as rank deficiency and it can be removed in some circumstances when the analysis is performed simultaneously on multiple experiments where the species concentration profiles show different patterns due to the different initial experimental conditions (rank augmentation by matrix augmentation) (Izquierdo-Ridorsa et al., 199; 7Amrhein et al., 1996; Norgaard and Ridder, 1994). In the present work, photodegradation of AML at different pH values was investigated by MCR-ALS analysis of UV spectrophotometric data. The degradation experiments were computed together with acid-base titration experiments. Two hard-modelling constraints, both based on non-linear fitting routines of the resolved concentration profiles and able to fulfil the acid-base equilibrium and the kinetic photodegradation pathway, were proposed.

3.3.1. *Materials and experimental procedures.*

a.   *Chemicals and instruments*

AML was purchased from Sigma-Aldrich Co. (Italy). A Crison pH-meter GPL 22 (Crison, Spain) was used to monitor the pH during the photodegradation and titration experiments.

Light exposure was performed in a light cabinet Suntest CPS+ (Heraeus, Italy), equipped with a Xenon lamp, able to closely simulate sunlight and to select spectral regions by interposition of appropriate filters.

Spectrophotometric measurements were recorded using an Agilent 8453 Diode Array spectrophotometer (Agilent Technologies, CA, USA).

b. Experimental procedures

Spectrophotometric acid-base titration were performed on solutions at different AML concentrations (10, 20 and 30 mg L^{-1}), in a 2 M NaOH solution. The samples were titrated from pH 12 to pH 1 using a 6 M HCl solution. This high concentration of HCl produced a negligible dilution effect on species concentrations. The UV spectra were stored every 0.5 pH increment giving a number of 20-25 spectra for every acid-base titration.

A stock solution of AML (1 g L^{-1}) in water was properly diluted to obtain four samples (30 g L^{-1}) at pH values of 3.0, 7.0, 9.0 and 12.0 by addition of HCl or NaOH. These samples, in quartz cells perfectly stoppered, were light irradiated according to the ID65 standard of the ICH rules.[18] The wavelength range was set between 300 and 800 nm, by means of a glass filter and the irradiation power was fixed at 550 W m^{-2}, corresponding to the energy value of 33 kJ (min m^2)$^{-1}$. The inner temperature was maintained constant at 25 °C in all the experiments. UV spectra were recorded in the wavelength range of 200-450 nm, just after sample preparation (t = 0 min) and every 5 min of photodegradation treatment, up to 360 min. A total number of about 70 spectra were stored in each photodegradation experiment.

c.   Data handling

UV-visible ChemStation software supplied with the Spectrophotometer (Agilent Technologies, CA, USA) and Masslynx supplied with Mass Spectrometer (Micromass, UK) were used for control, data acquisition and initial data pre-processing. DataBridge was the file converter provided with Masslynx to convert LC-MS raw files into an ASCII format. All chemometric analysis was performed under Matlab® computer environment (Mathwork Inc., version 7). MCR-ALS and HS-MCR-ALS routines computer methods were implemented as MATLAB functions. They were used as described in literature (de Juan et al., 2009; de Juan et al., 2000). Source files containing these algorithms are available by visiting the web site "www.mcrals.info".

3.3.2   Chemometric techniques

In this work, UV spectrophotometric data matrices from photodegradation experiments on AML, performed under different pH values, were simultaneously analysed together with the UV data matrices obtained in acid-base titration of AML solutions at three concentration levels. These data sets were arranged in a column-wise augmented data matrix consisting of a total number of seven different spectrophotometric data matrices and analysed by MCR-ALS algorithm, four from the photodegradation experiments and three from the acid-base titration. The following matrix equation (in MATLAB notation) summarizes the bilinear model applied to this multi-experiment data system:

1) $\mathbf{D}_{aug} = [\mathbf{D}_{d3};\mathbf{D}_{d7};\mathbf{D}_{d9};\mathbf{D}_{d12};\mathbf{D}_{t10};\mathbf{D}_{t20};\mathbf{D}_{t30}] = [\mathbf{C}_{d3};\mathbf{C}_{d7};\mathbf{C}_{d9};\mathbf{C}_{d12};\mathbf{C}_{t10};\mathbf{C}_{t20};\mathbf{C}_{t30}]\mathbf{S}^{T}$ **+** $[\mathbf{E}_{d3};\mathbf{E}_{d7};\mathbf{E}_{d9};\mathbf{E}_{d12};\mathbf{E}_{t10};\mathbf{E}_{t20};\mathbf{E}_{t30}] = \mathbf{C}_{aug}\mathbf{S}^{T} + \mathbf{E}_{aug}$

where $\mathbf{D}_{di}$ are the spectrophotometric data matrices corresponding to the AML photodegradation experiments at pH 3, 7, 9, 12 and $\mathbf{D}_{tj}$ are the individual spectrophotometric data matrices corresponding to the acid-base titration with AML at 10, 20 and 30 mg L^{-1}. The MATLAB semicolon notation ';' indicates that every individual data matrix $\mathbf{D}_{di}$ or $\mathbf{D}_{tj}$ obtained in a different experiment is arranged one on top of the other, keeping the same number of columns (wavelengths) in common, and consequently increasing the number of spectra rows of the corresponding augmented matrix $\mathbf{D}_{aug}$. Only one spectral matrix $\mathbf{S}^T$ is resolved for all the data submatrices, which forces spectra of the same components to be common for the different simultaneously analysed matrices. In contrast, each concentration profile matrix ($\mathbf{C}_{di}$ or $\mathbf{C}_{tj}$) is coupled to a different kinetic ($\mathbf{D}_{di}$) or equilibrium ($\mathbf{D}_{tj}$) experiment and the concentration profiles of the same component in the different matrices can be modelled independently (Garrido et al., 2005; Leger and Wentzell, 2002).

a. Hybrid hard- and soft- multivariate curve resolution (HS-MCR-ALS) methods

HS-MCR-ALS methods are a further step to solve some limitations of pure hard- and pure soft-modelling methods in the study of complex chemical processes and to improve resolution of the species profiles. These methods reduce the possible rotational ambiguities associated with the soft-modelling curve resolution, allowing to achieve unique solutions when the correct chemical model is chosen (de Juan et al., 2000). HS-MCR-ALS modelling has a high flexibility on the selection of which species are submitted to the fulfilment of the kinetic or equilibrium model.

Two different mixed hard soft modelling procedures were used in this work to constraint MCR-ALS solutions to fulfil respectively the proposed kinetic and equilibrium models (Maeder and Neuhold, 2007; Maeder and Zuberbuhler, 1990).

These constraints were applied in ALS iterations, giving the corresponding rate or acid-base equilibrium constants of the considered reaction system as additional valuable chemical information (De Luca et al., 2011; De Luca et al., 2010). Details about implementation of these two constraints, kinetic and acid-base equilibrium, have been given in previous works (Maeder and Neuhold, 2007; Maeder and Zuberbuhler, 1990). In both cases, the calculation involves the use of non-linear curve fitting routines to iteratively fit the concentration profiles resolved by MCR-ALS whit the optimal kinetic rate or equilibrium constant.

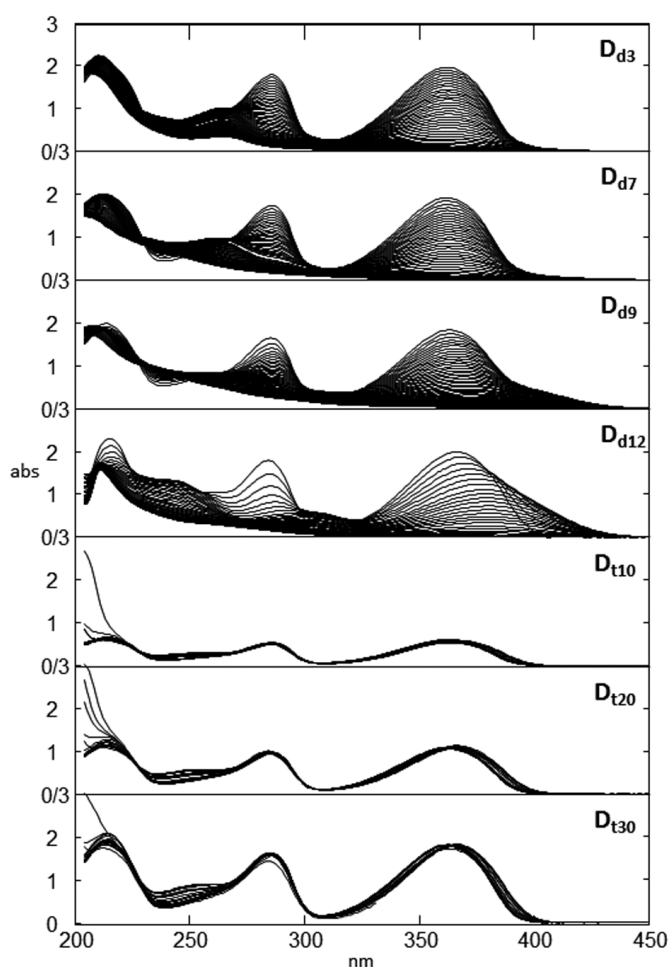### 3.3.3.   *Experimental results and discussion*

a.   *Soft modelling MCR-ALS*

Figure 3.10 - UV-spectra of photodegradation experiments (D_{d3}, D_{d7}, D_{d9} and D_{d12}) and titration experiments (D_{t10}, D_{t20} and D_{t30}).

Data collected during the spectrophotometric photodegradation experiments at four pH values (pH = 3, 7, 9 and 12) produced the set of matrices D_{d3}, D_{d7}, D_{d9}, and D_{d12} (Fig. 3.10). The spectra showed that the degradation at these pH values gave different spectral features and evolution. Moreover, the spectra before starting degradation presented different shapes, due to formation of ionized and non-ionized AML at different pH values.

The study of the AML photodegradation system is very complex, because acid-base equilibrium and photodegradation process are simultaneously involved and the additional presence of chemical rank deficiencies make more difficult the full resolution of all involved species and the understanding of the underlying reactions. With the purpose to reduce rank deficiency problems and describe adequately the acid-base equilibrium system of AML simultaneously to its photodegradation, matrices D_{t10}, D_{t20}, D_{t30}, from UV spectrophotometric titrations on AML at three concentration levels (Fig. 3.10), were analysed simultaneously to the matrices from the photodegradation experiments previously described. Table 3.3 lists the estimation of the number of species involved in the photodegradation and titration experiments and the results from analysis on the single matrices and on the augmented data matrices containing the photodegradation kinetic experiments ($D_{aug1}=[D_{d3};D_{d7};D_{d9};D_{d12}]$) and both the photodegradation and titration experiments ($D_{aug2}=[D_{d3};D_{d7};D_{d9};D_{d12};D_{t10};D_{t20};D_{t30}]$).

Table 3.3 - Estimation of the number of components (rank analysis via SVD) and MCR-ALS results from analysis on single and augmented data matrices.

Experimental data matrices	N. components by SVD	AML/AMLH+ resolution	Number of photoproducts in MCR-ALS resolved concentration profiles			
			C_{d3}	C_{d7}	C_{d9}	C_{d12}
D_{d3}	4	Yes	3	-	-	-
D_{d7}	4	Yes	-	3	-	-
D_{d9}	4	Not	-	-	3	-

$\mathbf{D}_{d12}$	3	Yes	-	-	-	2
$\mathbf{D}_{t10}$	2	Yes	-	-	-	-
$\mathbf{D}_{t20}$	2	Yes	-	-	-	-
$\mathbf{D}_{t30}$	2	Yes	-	-	-	-
$\mathbf{D}_{aug1}=[\mathbf{D}_{d3};\mathbf{D}_{d7};\mathbf{D}_{d9};\mathbf{D}_{d12}]$	7	Not	2	2	3	2
$\mathbf{D}_{aug2}=[\mathbf{D}_{d3};\mathbf{D}_{d7};\mathbf{D}_{d9};\mathbf{D}_{d12};\mathbf{D}_{t10};\mathbf{D}_{t20};\mathbf{D}_{t30}]$	8	Yes	3	3	3	2

The singular value decomposition (SVD) of each data matrix gave estimation of four different components for the experiments performed at pH 3, 7 and 9, and of three components for the experiment at pH 12. The respective MCR-ALS analyses of the individual experiments gave, however, only a partial resolution of the corresponding photoproducts. In particular, no resolution of the AML acid-base system was achieved for the experiment at pH 9, where MCR-ALS analysis was unable to distinguish the two AML forms (protonated and unprotonated). Therefore, the number of the resolved species resulted to be clearly lower than the real number of different absorbing species.

The simultaneous analysis of the photodegradation experiments at different pH values (in the column-wise augmented data matrix) was not either able to resolve all the species involved. Rank analysis of this augmented matrix suggested the presence of seven components, but the results obtained by MCR-ALS did not resolve properly the interaction between the kinetic and equilibrium systems. In submatrices $\mathbf{C}_{d3}$ and $\mathbf{C}_{d7}$, one of the components previously resolved in the individual analysis of kinetic experiments, was lost, and in submatrix $\mathbf{C}_{d9}$, the two AML/AMLH$^+$ species were poorly resolved. Finally, rank analysis of the augmented matrix containing both photodegradation and titration experiments gave eight components. In this case, the simultaneous MCR-ALS analysis of both kinetic and equilibrium systems (see equation 1), using non-negativity, unimodality and closure constraints, gave more satisfactory results, with the $\mathbf{C}_{aug2}$ and $\mathbf{S}^T$ matrices shown in figure 3.11.
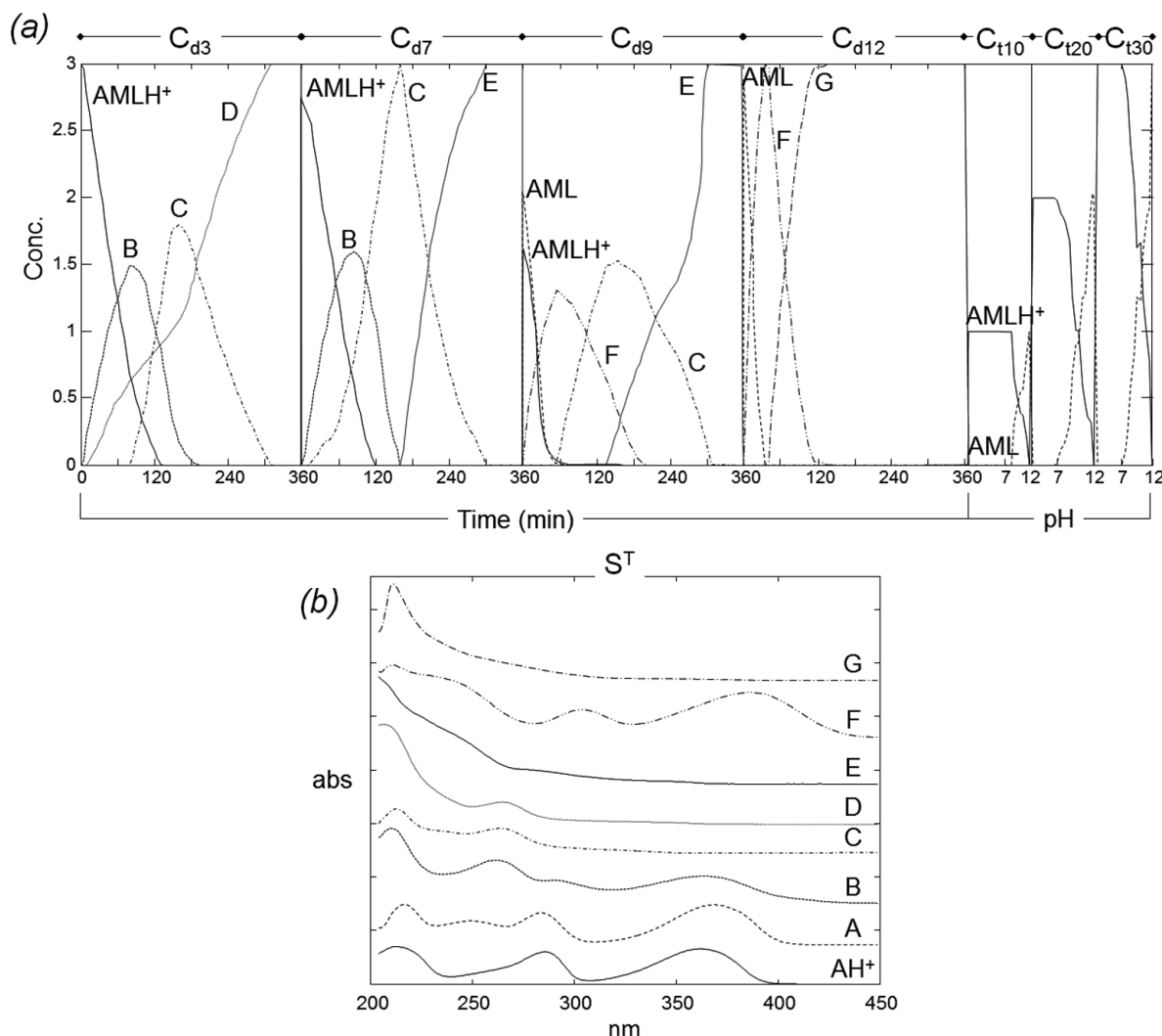
Figure 3.11 - Concentration profiles (a) and pure spectra (b) obtained by Soft-MCR-ALS analysis on augmented matrix from photodegradation and titration experiments (D_{aug2}); species B, C, D, E, F and G are the AML photoproducts.

Photodegradation concentration profiles resolved in submatrices C_{d3}, C_{d7}, C_{d9}, and C_{d12} showed clearly the dependence of the photodegradation process on pH. In agreement with these resolved concentration profiles and the corresponding resolved pure spectra, a preliminary speciation mechanism could be proposed for the photodegradation at each pH.

At pH 3, submatrix C_{d3} showed concentration profiles of four different species: the protonated AMLH$^+$ and three its photoproducts, formed according to three

consecutive reactions, with a mechanism postulated as $AMLH^+>B>C>D$. At this pH, the unprotonated form of AML is not present. At pH 7, submatrix $\mathbf{C}_{d7}$ gave quite similar concentration profiles to $\mathbf{C}_{d3}$, except that the last species D, replaced by a new species E (with a different spectrum than D) with a mechanism $AMLH^+>B>C>E$. At this pH, the unprotonated form of AML does not either exist. At pH 9, the photoproducts in submatrix $\mathbf{C}_{d9}$ changed with B replaced by a new species F, following a new possible mechanism $AML/AMLH^+>F>C>E$. It is noteworthy that in this case, at the starting of degradation, the mixture of the protonated and unprotonated AML were properly resolved and suffered simultaneous degradation. Therefore, the degradation products should probably come from both AML species, although they could not be separated (B was no longer detected while F appeared). Finally, at pH 12, submatrix $\mathbf{C}_{d12}$ showed different species. Previous species B, C and E were not present anymore and E was substituted with G, following the possible mechanism $AML>F>G$. At this pH, only the unprotonated AML was present.

In the resolution of the titration experiments ($\mathbf{C}_{t10}$, $\mathbf{C}_{t20}$, and $\mathbf{C}_{t30}$ matrices), the concentration profiles of the two AMLH/AML acid-base pair species followed the expected dependence on pH and on drug concentration. The pKa value was deduced from the pH close to 8.7, where concentration profiles of AML and $AMLH^+$ crossed ($[AML]=[AMLH^+]$). Coupling of the two reaction systems, AML acid-base equilibria and AML photodegradation kinetics, was properly resolved from MCR-ALS, where photodegradation involved either AML or $AMLH^+$ or both the species, depending on pH (Fig. 3.11a).

In summary, application of soft modelling MCR-ALS allowed the preliminary resolution of the complex reaction system described above without proposing any initial model for the chemical speciation. The results already suggested the common and different species formed during the photodegradation experiments at different

pH values, allowing a rough preliminary interpretation of the chemical model. The models based on the constraints mass action and rate laws could be so postulated for equilibrium and for all kinetic systems.

b.   *Acid-base equilibrium constraint on concentration profiles (E-HS-MCR-ALS)*

The mixed hard and soft MCR-ALS method was first used for the analysis of titration and kinetic experiments, adopting the equilibrium constraint (E-HS-MCR-ALS) during the ALS optimization of concentration. In this analysis, the spectral data from the acid-base titration D_{tj}, and from the photodegradation experiments at different pH values D_{di}, were simultaneously analysed in the augmented matrix D_{aug2}, but they were constrained differently, as listed in Table 3.4.

Table 3.4 - Parameters and results of the analysis on D_{aug2} by using HS-MCR-ALS

Resolution of D_{aug2} by using the equilibrium constraint. (%LOF = 2.24)

Submatrices in D_{aug}	Parameters			Results	
	MCR-ALS constraints*	Fixed C_A (mg L^{-1})	Optimized pKa	[AMLH$^+$] x_i**	[AML] x_i**
D_{d3}	N, U, C			0.9990	0.0011
D_{d7}	N, U, C			0.8520	0.1480
D_{d9}	N, U, C			0.3153	0.6857
D_{d12}	N, U, C			0.0032	0.9989
D_{t10}	E-HS, N	10.00	8.709±0.0015		
D_{t20}	E-HS, N	20.00	8.699±0.0012		
D_{t30}	E-HS, N	30.00	8.685±0.0029		

Resolution of D_{aug2} by using the kinetic constraint.(%LOF = 4.52)

	MCR-ALS constraints*	Optimized ki (x10^{-3})		
D_{d3}	K-HS, N, U	$k_{A>B}$= 11.11±0.25	$k_{B>C}$= 4.99±0.09	$k_{C>D}$ =15.41±0.18

D_{d7}	K-HS, N, U	$k_{A>B}= 12.13\pm0.01$	$k_{B>C}= 5.99\pm0.02$	$k_{C>E}=21.14\pm0.58$
D_{d9}	K-HS, N, U	$k_{A>F}= 15.56\pm0.54$	$k_{F>C}= 6.16\pm0.15$	$k_{C>E}=28.43\pm0.63$
D_{d12}	K-HS, N, U	$k_{A>F}= 20.81\pm0.48$	$k_{F>G}=35.81\pm0.58$	
D_{t10}	N, U, C			
D_{t20}	N, U, C			
D_{t30}	N, U, C			

*E-HS = equilibrium constraint in hybrid HS-MCR-ALS, K-HS = kinetic constraint in hybrid HS-MCR-ALS, N = non-negativity, U = unimodality and C = closure constraints
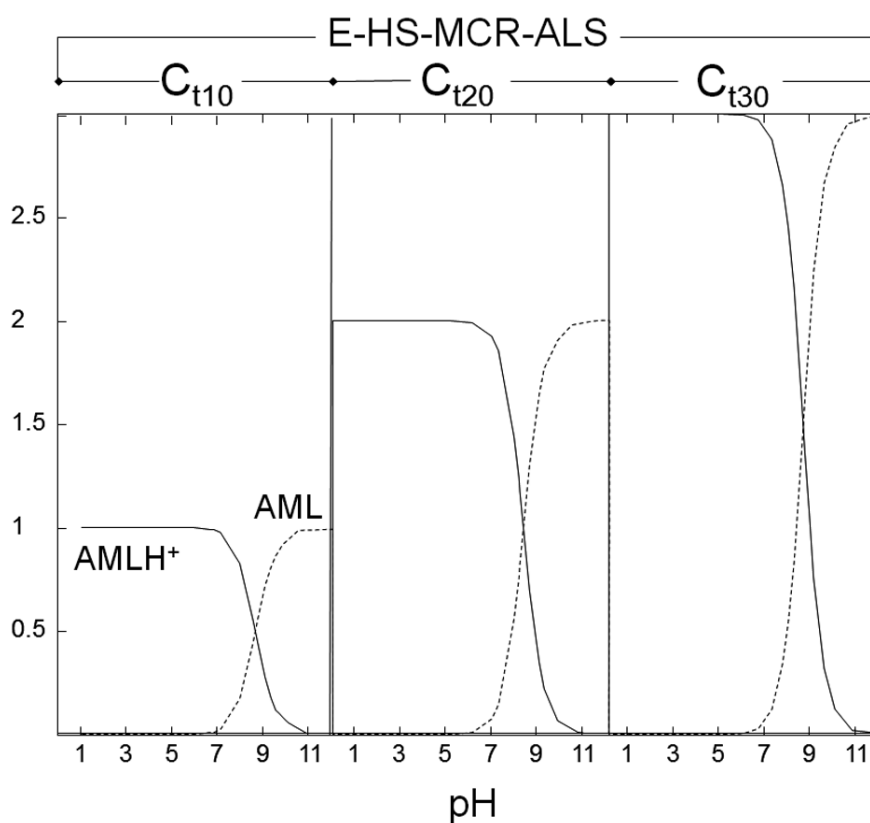** [AMLH+] and [AML] are reported as mole fraction ($x_i=n_i/n_{tot}$)

Figure 3.12 - Concentration profiles obtained by E-HS-MCR-ALS analysis on titration experiments.

The acid-base equilibrium constraint was applied only to the sub-matrices from titration, while sub-matrices from degradation experiments were analysed by soft MCR-ALS analysis. This procedure permitted the estimation of the concentration profiles of AML and AMLH+ in both titration and degradation experiments. Figure 3.12 shows the concentration profiles resulted from E-HS-MCR-ALS analysis on

AML titration data, table 3.4 lists the AML pKa values and the initial concentrations of AML and AMLH$^+$ estimated for each photodegradation experiment. These values were afterwards used as starting concentrations in the next kinetic HS-MCR-ALS application.

       c.   *Kinetic constraint on concentration profiles (K-HS-MCR-ALS)*

A further HS-MCR-ALS type of modelling was performed for the simultaneous analysis of titration and kinetic experiments using the kinetic modelling constraint during the ALS optimization of concentration profiles (K-HS-MCR-ALS). In this case, all submatrices in matrix D_{aug2} were simultaneously resolved, but only the

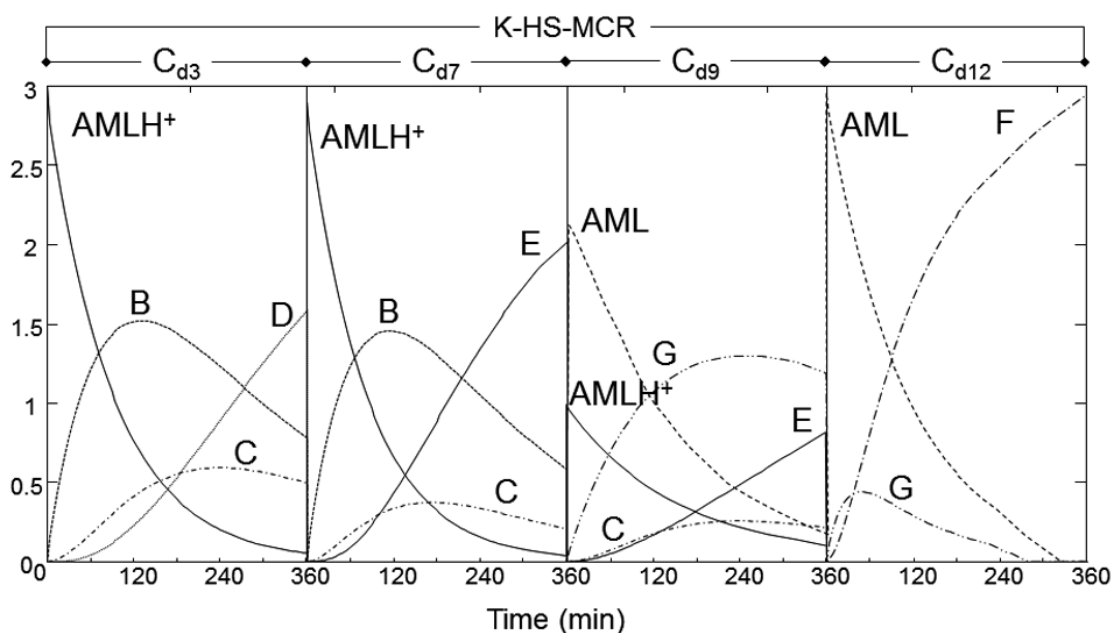*Figure 3.13 - Concentration profiles obtained by K-HS-MCR-ALS analysis on photodegradation experiments; species B, C, D, E, F and G are the AML photoproducts*

concentration profiles of the photodegradation experiments were constrained by the kinetic non-linear curve fitting routine, while those from titration were analysed by ordinary soft MCR-ALS approach. The starting concentration of AML and AMLH$^+$ at

different pH was fixed according to the results obtained in the previous E-HS-MCR-ALS analysis. Application of the kinetic constraint allowed the optimization of the concentration profiles in the photodegradation experiments, according to the selected models and the evaluation of the rate constants. K-HS-MCR-ALS results are shown in table 3.4 and in figure 3.13. Resolved pure spectra of all species were practically equal to those obtained by soft MCR-ALS modelling, but the concentration profiles showed better shapes, in agreement with the proposed kinetic pathways and the obtained rate constants, allowing a better evaluation of the influence of pH on the AML photodegradation. When a particular reaction was present in more than one photodegradation experiment, the values of the rate kinetic constants highlighted the dependence on pH, increasing when pH values also increased. Again, the simultaneous resolution of $AMLH^+$ and AML, depending on the starting pH, was achieved, describing more accurately the photodegradation experiment at pH 9, where the two species were simultaneously present at similar concentrations.

3.4. **Multivariate curve resolution of incomplete fused multiset data from chromatographic and spectrophotometric analyses for drug photostability studies**

Photodegradation kinetic experiments can be performed in different ways and monitored by various analytical and instrumental approaches (Ragno et al., 2006a; Calza etal., 2008). Spectrophotometric analytical procedures are particularly attractive because of the simplicity, short analysis time and low cost with nearly no sample preparation required. In particular, UV spectrophotometry can be used to follow the evolution of UV absorbing species involved in a kinetic reaction. In this case, the sequential spectra are collected as a function of time and analyzed by appropriate chemometric tools (Ragno et al., 2006b; Calza et al., 2008; Ragno et al., 2006). Unfortunately, UV spectrophotometry suffers from sensitivity in determining low concentrations and of lack of selectivity in identifying the involved species. For this reason, although UV spectral data from photodegradation experiments provide very precise data for quantitative purposes, they should be conveniently combined with those from other analytical techniques having larger sensitivity and selectivity. Chromatographic methods coupled to spectrometric detection methods seem to be the more appropriate for this purpose (De Luca et al., 2012).

Chemometric procedures such as multivariate curve resolution (MCR) have proved to be suitable for the simultaneous investigation of the analytical information coming from different experiments and/or analytical methods (Smilde et al., 2004; Bro, 1997). In particular, the MCR-ALS method has been successfully adopted for the analysis of multisets and multiway data (Tauler et al., 2009; Mas et al., 2008; A. de Juan and Tauler, 2001; Tauler et al., 1998). Possible rotation ambiguities associated with the resolved MCR profiles can be considerably reduced and often eliminated

when data multisets are simultaneously analyzed and some constraints such as trilinearity, quadrilinearity or interaction between components are applied (Malik and Tauler, 2013; Alier et al., 2011; De Luca et al., 2010; Peré-Trepat et al., 2007) However, when data from different instrumental methods and different approaches are combined, the resulting fused data may not have the adequate full complete structure required for the application of multiway methods nor for the traditional MCR-ALS analysis of row-wise, column-wise or row- and column-wise augmented matrices (Mas et al., 2008).

In the case of photostability kinetic studies, experiments may be performed in different conditions and monitored by different analytical methods, producing data blocks that cannot be arranged in complete datasets. Moreover, the presence of missing data blocks can occur by other causes, such as bad working of instruments, partially successful experiments or limited data acquisition of signals due to high noise levels (Acar et al., 2011).

AML is a potassium-sparing diuretic agent, widely used in combination with hydrochlorothiazide, for the treatment of hypertension (Vidt, 1981). Adverse photosensitivity reactions in patients, observed as an exaggerated sunburn like reaction to sunlight, has been reported among the side effects associated with this formulation. AML light stability has been already investigated in my previous work (De Luca et al., 2012), in which the kinetic pathway of AML degradation was preliminary studied by applying MCR to the UV spectrophotometric data, and by other authors (Li et al., 1999). Nevertheless, these studies were able to give only partial knowledge about the rather complex analytical system, characterized by multiple unknown species formed during the photodegradation process.

Photostability of AML has been studied from several points of view, but the experimental results have never been processed simultaneously to give a

comprehensive description of the whole degradation process. In this work, a new version of MCR-ALS has been tailored for the analysis of incomplete data sets collected from different experiments and analytical techniques, applied to AML photodegradation experiments (Alier and Tauler, 2013; ICH, 1996). UV spectrophotometric kinetic experiments were coupled to chromatographic determinations using diode-array (DAD) and mass spectra (MS) detectors. In this data fusion procedure, UV and LC-DAD provided the bridge between UV spectrophotometric acid-base and kinetic experiments on one hand and LC-MS on the other hand.

The whole data set (UV titration and kinetic experiments together with LC-DAD and LC-MS experiments) was combined in a data structure built by an incomplete column- and row-wise augmented data matrix. Since AML stability is pH dependent, acid-base titration experiments were coupled to kinetic degradation and chromatographic experiments (with DAD and MS detection).

3.4.1. *Materials and experimental procedures.*

a. *Chemicals and instruments*

AML was purchased from Sigma-Aldrich Co. (Italy); formic acid, hydrochloric acid, sodium hydroxide (all of analytical grade) and methanol (HPLC-grade) were supplied by Merck (Germany). Water, with a conductivity <0.05 μS cm^{-1}, was obtained using a MilliQ water purification system (Millipore, France).

A Crison pH-meter GPL 22 (Crison, Spain) was used to monitor the pH during the photodegradation and titration experiments. Light exposure was performed in a light cabinet Suntest CPS+ (Heraeus, Italy), equipped with a Xenon lamp, able to

closely simulate sunlight and to select spectral regions by interposition of appropriate filters.

Spectrophotometric measurements were recorded using an Agilent 8453 Diode Array spectrophotometer (Agilent Technologies, CA, USA). Chromatographic equipment consisted of a Waters 2690 series Alliance HPLC (Waters, MA, USA) coupled to a mass spectrometer (MS) detection system. The analytes were separated on a 250×4 mm, I.D. 5 μm RP18 LiChrospher 100 column (Merck, Germany). The sample injection volume was set at 30 μL. A binary isocratic mobile phase with 80% of formic acid (0.05% in water) and 20% methanol was used at a flow rate of 1.0 mL min^{-1}. Within the DAD/MS detection system, MS detection was carried out on a bench top triple quadrupole mass spectrometer Quattro LC from Micromass (UK) with APCI (atmospheric pressure chemical ionization) interface at the following conditions: capillary voltage −3.5 kV, cone voltage −40 V, source and desolvation temperature 120 °C. The MS detector operated in scan mode (40–260 amu, Δamu = 1) with scan duration of 1 sec scan^{-1} and an interscan time of 0.1 sec. The DAD detection in the UV range was fixed at a spectral resolution of 1.2 nm in the spectral range from 200 to 450 nm, collecting one spectrum per second.

b.   Experimental procedures.

Spectrophotometric acid-base titrations were performed on solutions at different AML concentrations (10, 20 and 30 mg L^{-1}), in a 2 M NaOH solution. The samples were titrated from pH 12 to pH 1 using a 6 M HCl solution. This high concentration of HCl produced a negligible dilution effect on species concentrations. The UV spectra were stored every 0.5 pH increment giving a number of 20-25 spectra for every acid-base titration.

A stock solution of AML (1 g L^{-1}) in water was properly diluted to obtain four samples (30 mg L^{-1}) at pH values of 3.0, 7.0, 9.0 and 12.0 by addition of HCl or NaOH. These samples, in quartz cells perfectly stoppered, were light irradiated according to the ID65 standard of the ICH rules (ICH, 1996). The wavelength range was set between 300 and 800 nm by means of a glass filter and the irradiation power was fixed at 550 W m^{-2}, corresponding to the energy value of 33 kJ (min m^2)$^{-1}$. The inner temperature was maintained constant at 25 °C in all the experiments. UV spectra were recorded in the wavelength range of 200-450 nm, just after sample preparation (t = 0 min) and every 5 min of photodegradation, up to 360 min. A total number of about 70 spectra were stored in each photodegradation experiment.

AML samples (at different pH values) for LC-MS/DAD analysis were irradiated in sealed quartz tubes (12.5x1.5 cm). Aliquots of 1 mL were taken just before irradiation (t = 0 min) and every 20 min up to 360 min. 70 samples for each photodegradation experiment were submitted to LC-DAD/MS analysis.

c.   Data handling.

UV-visible ChemStation software supplied with the Spectrophotometer (Agilent Technologies, CA, USA) and Masslynx supplied with the Mass Spectrometer (Micromass, UK) were used for control, data acquisition and initial chromatographic data pre-processing. DataBridge was the file converter provided with Masslynx to convert LC-DAD-MS raw files into an ASCII format. Chemometric analysis was performed under Matlab® computer environment (Mathwork Inc., version 7). MCR-ALS computer methods were implemented as MATLAB functions. They were used as described in previous works (see also details below about its implementation for incomplete data sets) (Alier et al., 2011). Source files containing these algorithms are available by visiting the web site "www.mcrals.info". The new MCR-ALS command

line in MATLAB to work with incomplete data is a recent homemade version only available at present under request to one of the authors.

In order to process simultaneously chromatographic DAD and MS data, preliminary pre-processing procedures were needed. The two detection systems in tandem were subjected to a short time delay on peak signal recording, due to the transfer tubing between DAD (first) and MS (second) detectors. This time delay was calculated to be 0.2020 min and it was removed by erasing the mass spectra recorded at the beginning of the chromatogram, in the time interval 0-0.2020 min. Moreover, another data pretreatment was needed because of different frequency in spectra acquisition by the two detectors. During the chromatographic elution, the DAD detector had higher recording frequency and then a higher number of UV spectra was acquired than the MS spectra. MATLAB function "interp1" for linear interpolation was then used to synchronize DAD and MS detector signals and match them in the time direction of the analyzed data matrices.

d.   Data arrangement.

The data sets analyzed in this work were produced by three types of different experimental procedures. A detailed description of how these data sets were arranged for their simultaneous analysis is given in figure 3.14 and described below.

A) The first data set was obtained from acid-base titrations of AML at 3 different concentrations (10, 20 and 30 mg L^{-1}). These three UV titration data sets gave three data matrices (D_{tj}), where their rows had the measured UV spectra (absorbance at 246 wavelengths in the range 205-450 nm) recorded at different pHs during the titration experiments (spectra vs pH), D_{t10} (19 x 246), D_{t20} (18 x 246), D_{t30} (18 x 246).

B) The second data set was produced during AML photodegradation experiments at four different pH values (3.0, 7.0, 9.0 and 12.0): UV kinetic data sets gave four

matrices D_{di}, where their rows had the measured UV spectra recorded at different time intervals during the kinetic degradation process (spectra vs reaction time), D_{d3} (73 x 246), D_{d7} (67 x 246), D_{d9} (54 x 246), D_{d12} (49 x 246).

C) The third data set was larger and much more complex and was obtained during chromatographic analysis of AML kinetic photodegradation experiments at the four different pHs (3.0, 7.0, 9.0 and 12.0). As described in the experimental procedure, at preselected reaction times, aliquot samples from the kinetic photodegradation experiment were submitted to LC analysis. At every LC analysis, two large data matrices were obtained from DAD and MS detection systems, D_{DADn} and D_{MSn}. In these matrices, rows were the UV and MS spectra recorded at different elution times (431 DAD and 431 MS spectra in the elution time interval 1.331-8.7130 min) and columns were the chromatographic elution profiles recorded at different wavelengths (246 wavelengths in the range 205-450 nm) and at different m/z values (200 MS intensity signals in the range 40-239 m/z), respectively.

A considerable number of samples at different reaction times and pH values were submitted to chromatographic analysis and large DAD and MS chromatographic data matrices were acquired. They were organized in the way described in figure 3.14. D_{DAD3} is the column-wise augmented data matrix formed by 20 data submatrices, one at every photodegradation time sampling, with dimensions 431 x 246. In the same way, the other three augmented data DAD matrices were arranged in 20 new data submatrices at the corresponding 20 reaction times, with dimensions 431 x 246 for D_{DAD7}, 19 new data submatrices of dimensions 431 x 246 for D_{DAD9} and 19 new data submatrices of dimensions 431 x 246 for D_{DAD12}. The dataset from MS detector consisted on 4 augmented data matrices, D_{MS3} with 20 sub matrices of dimensions 431 x 200, D_{MS7} with 20 new data submatrices of dimensions 431 x 200, D_{MS9} with

19 new data submatrices of dimensions 431 x 200, D_{MS12} with 19 new data submatrices of dimensions 431 x 200. All these data matrices were finally grouped (see Figure 3.14) in the row- and column wise super augmented matrix, D_1 (D_1=[[D_{DAD3};D_{DAD7};D_{DAD9};D_{DAD12}],[D_{MS3};D_{MS7};D_{MS9};D_{MS12}]]). On the other hand, all matrices which share the UV spectra vectorial space (columns of the matrices), which include data sets from titration and photodegradation experiments as well as from DAD chromatographic detection experiments, were grouped in column-wise super augmented data matrix D_2 (D_2=(D_{t10};D_{t20};D_{t30};D_{d3};D_{d7};D_{d9};D_{d12};D_{DAD3};D_{DAD7};D_{DAD9};D_{DAD12}). Grouping D_1 and D_2, gave finally the row- and column wise hyper augmented incomplete data set D_{aug}. Since only matrices from titration and kinetic experiments, D_{tj} and D_{di}, had only the UV spectra blocks and were lacking MS blocks, D_{aug} was said incomplete. In order to complete a squared data matrix structure and to identify the incomplete data blocks in MATLAB environment, all missing blocks were filled with the MATLAB NaN (Not a Number) notation for missing values.

In a previous study (Paragraph 3.3; De Luca et al., 2010), two of the data sets previously analyzed were similar to those investigated in this work, one related with titration data D_{tj}, and another one related with the UV spectrophotometric kinetic data, D_{di}. They were preliminarily analyzed using the MCR-ALS procedure, firstly separately, and then jointly using a column-wise data matrix arrangement. In this previous study, MS data was only analyzed via traditional methods to identify possible species involved in the kinetic process, without using any further multivariate data analysis.

3.4.2. MCR-ALS method for incomplete data sets.

In a photodegradation study, where the kinetic process is often unknown and many species can be involved, the determination of the number of independent components is an important step. Singular component decomposition analysis may identify a lower number of components than the real number of absorbing species if their concentration or spectral (response) profiles are linearly dependent. This produces a chemical rank deficiency (mathematical rank in absence of noise) due to the linear dependence of the concentration or spectra profiles in the system. Nevertheless, the simultaneous analysis of multiple experiments under different
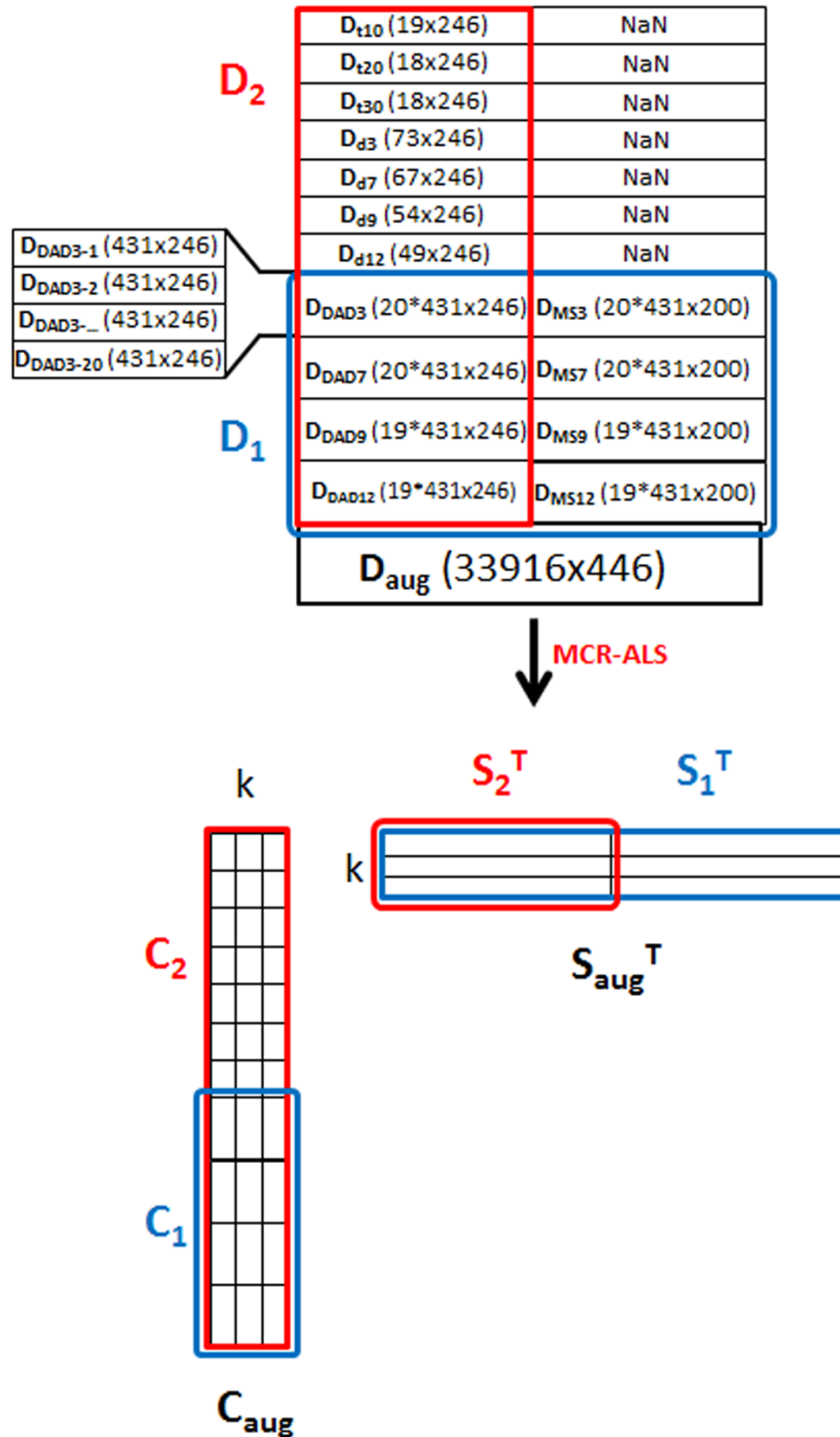
Figure 3.14 - MCR-ALS method for incomplete data sets. "NAN" is the MATLAB notation for missing values.

conditions and/or analysed by different instrumental methodologies, via row-wise, column-wise or row- and column-wise data matrix augmentation, can remove rank deficiency problems, allowing estimation of the correct number of components and

resolution of the whole system (de Juan and Tauler, 2006. Moreover, as reported in previous works (De Luca et al., 2012; Calza et al., 2008), a clear identification of the species involved in a complex degradation chemical system needs coupling of classical kinetic studies by spectrophotometry with other more sophisticated detections systems, such as mass spectrometry, coupled to chromatographic separation.

The MCR-ALS procedure proposed in this work was applied to the analysis of the incomplete data multiset shown in Figure 3.14. This multiset is constituted by two complete submatrices. D_1 is a wide row- and column-wise augmented data matrix with the chromatographic data from DAD and MS detectors and D_2 is a very long column-wise augmented data matrix which includes on one side the acid-base titration and kinetic photodegradation UV data and on the other side the LC-DAD data. Column-wise augmentation was possible in this case because UV spectral resolution was coincident for the three types of data matrices: titration, kinetic and LC-DAD data. Observe that D_1 and D_2 share the chromatographic UV-DAD data blocks, and that in the data decomposition of D_{aug}, C_1 is shared in C_{aug} and S_2^T is shared in S_{aug}^T (see figure 3.14). MCR bilinear decomposition of the matrices D_1 and D_2 can be performed either in a separate or in a simultaneous way, by using a new implementation of the popular ALS algorithm.[19]

This new MCR-ALS procedure, designed to resolve incomplete data multisets such as the one arranged in D_{aug}, uses different least squares error functions, one for each of the two augmented complete data matrices previously defined, D_1 and D_2. These two functions are optimised simultaneously (summing the two individual error functions in a total error function) to find out an optimal estimation of concentration and spectral profiles describing simultaneously all included data sets. In this bilinear

decomposition of $\mathbf{D_1}$ and $\mathbf{D_2}$ according to Equation 1, concentration matrix $\mathbf{C_1}$ has the same rows as $\mathbf{D_1}$, concentration matrix $\mathbf{C_2}$ has the same rows as $\mathbf{D_2}$. Pure spectra $\mathbf{S_1^T}$ has the same columns of $\mathbf{D_1}$, whereas pure spectra $\mathbf{S_2^T}$ has the same columns of $\mathbf{D_2}$.

Missing data blocks (data matrices) can be estimated from final results. In the calculation of the concentration matrices from the incomplete data set, two different situations are encountered: a) evaluation of the matrix $\mathbf{C_1}$ from data matrix $\mathbf{D_1}$ which accounts for the data corresponding only to the common DAD and MS data, (b) evaluation of the matrix $\mathbf{C_2}$ from data matrix $\mathbf{D_2}$ which accounts only for the data corresponding to UV and DAD data. In every case, the calculation involves the multiplication of the appropriate augmented data matrix, $\mathbf{D_1}$ or $\mathbf{D_2}$, by the pseudoinverse of the corresponding spectrum profiles matrix, $\mathbf{S_1^T}$ and $\mathbf{S_2^T}$. In figure 3.14, appropriate rows and columns of the incomplete data matrix will be selected to form two rectangular invertible data submatrices and the resulting columns of the corresponding $\mathbf{S^T_{aug}}$ matrices will have the same number of the columns. Each iteration of ALS algorithm solves the following equations (Alier and Tauler, 2013):

By considering the data matrix $\mathbf{D_1}$, calculation of concentration matrix $\mathbf{C_1}$ by using the current estimation of $\mathbf{\hat{S}_1^T}$

2) $\quad \displaystyle\min_{\mathbf{\hat{C}_1},\text{constraints}} \left\| \mathbf{\hat{D}}_{1,\text{PCA}} - \mathbf{\hat{C}_1}\mathbf{\hat{S}_1^T} \right\| \quad \mathbf{\hat{C}_1} = fnnls(\mathbf{\hat{D}}_{1,PCA}, \mathbf{\hat{S}_1^T})$

and calculation of spectral matrix $\mathbf{S_1^T}$ from the present estimation of $\mathbf{\hat{C}_1}$ by

3) $\quad \displaystyle\min_{\mathbf{\hat{S}_1^T},\text{constraints}} \left\| \mathbf{\hat{D}}_{1,\text{PCA}} - \mathbf{\hat{C}_1}\mathbf{\hat{S}_1^T} \right\| \quad \mathbf{\hat{S}_1^T} = fnnls(\mathbf{\hat{D}}_{1,PCA}, \mathbf{\hat{C}_1^T})$

Where $\hat{\mathbf{D}}_{1,PCA}$ is the $\hat{\mathbf{D}}_1$ matrix projected on PCA model for the considered number of components. Evaluation of the least squares error function corresponding to data matrix $\mathbf{D_1}$ to be minimised which is defined from the residuals calculated by using the estimated $\hat{\mathbf{C}}_1$ of $\hat{\mathbf{S}}_1^T$.

$$4) \qquad ssq_1 = \sum_{i=1}^{I_1} \sum_{j=1}^{J_1} \left(d_{1,i,j}^2 - \sum_{n=1}^{N} \hat{c}_{1,i,n} \hat{s}_{1,j,n} \right)$$

In the same way, Equations 2-4 can be rewritten for the calculation of $\hat{\mathbf{C}}_2$ from $\hat{\mathbf{S}}_2^T$ and ssq_2 estimations corresponding to analysis of matrix $\mathbf{D_2}$.

The final $\hat{\mathbf{C}}_{aug}$ matrix is calculated by column-wise juxtaposition of the two concentration matrices

$$5) \qquad \hat{\mathbf{C}}_{aug} = \{\hat{\mathbf{C}}_1; \hat{\mathbf{C}}_2\}$$

when there are coincidences in the rows, matrix $\hat{\mathbf{C}}_1$ prevails over $\hat{\mathbf{C}}_2$ because $\mathbf{D_1}$ is the matrix that should contain more reliable information as it was obtained with the complete joint column vector space (Fig. 3.14). On the other hand, the corresponding final spectral matrix is estimated using the following equation

$$6) \qquad \hat{\mathbf{S}}^T_{aug} = \{\hat{\mathbf{S}}_1^{*T}, \hat{\mathbf{S}}_2^T\}$$

Where $\hat{\mathbf{S}}_1^{*T}$ is estimated as the average of the common parts of $\hat{\mathbf{S}}_1^{T}$ and $\hat{\mathbf{S}}_2^{T}$ (see figure 3.14) as $\hat{\mathbf{S}}_1^{*T} = \frac{1}{2}(\hat{\mathbf{S}}_1^{T}+\hat{\mathbf{S}}_2^{T})$ corresponding to the common columns of both $\mathbf{D}_1$ and $\mathbf{D}_2$ matrices.

The final equation optimised by ALS algorithm, is

7) $\quad sqq = sqq_1 + sqq_2$

from which the sigma value, σ, is estimated

8) $\quad \sigma = \sqrt{\dfrac{sqq}{(I_1 J_1 + I_2 J_2)}}$

Where I_1, J_1, I_2 and J_2 are the number of rows and columns in the matrices $\mathbf{D}_1$ and $\mathbf{D}_2$. In Eq. 8, σ gives the root mean square of the sum of the squares of the residuals (which are the differences between the experimental measured values and those calculated by the MCR-ALS method), ssq. The criterion of optimization convergence is reached when improvement on relative changes on this sigma value between iterations is below a threshold value, usually 0.1%. This value may be modified depending on the stage of the optimization.

An advantage of this method is its very flexible way to perform optionally a bilinear trilinear and mixed bilinear-trilinear model decomposition for some or for all the components of the system (Peré-Trepat et al., 2007; Jaumot et al., 2005; Tauler, 1995;). A more detailed description of this new variant of the MCR-ALS algorithm and of its application to bilinear and trilinear data decompositions has been recently reported by Alier et al., 2013

3.4.3. RESULTS AND DISCUSSION

MCR-ALS was first applied separately to the two complete data sets arranged in D_1 and D_2 augmented data matrices (see figure 3.14). Both D_1 and D_2 data matrices were then merged in the row- and column-wise incomplete augmented data matrix D_{aug}. A summary of the results of MCR-ALS application to these different data arrangements is given in table 3.5. Figure 3.15 shows resolution results (C_{aug} and S^T) achieved in the MCR-ALS analysis of the incomplete augmented data matrix D_{aug}. Eight components were finally resolved from the study of the complete augmented data matrices, D_1 and D_2. Up to six components explained the kinetic degradation at different pH values and the acid base equilibria of AML, while the other two components, were associated to instrumental variance and baseline chromatographic contributions, only present in the analysis of the chromatographic data.

Table 3.5. Statistical parameters obtained in MCR analyses.

Data matrix	%Lof	R^2
D_1	7.91	0.994
D_2	2.86	0.999
D_{Aug}	6.22	0.996

MCR-ALS analysis of augmented data matrices D_1 and D_2 gave good resolution results but explained the system only in a partial way. In the MCR-ALS analysis of the DAD-MS chromatographic augmented data matrix, D_1, the kinetic pathway of the degradation was described and the use of the two chromatographic detection systems allowed the identification of all AML photoproducts. However, no information

was achieved about the simultaneous AML acid-base equilibrium system and its speciation, and the chromatographic methods cannot be used for this aim, because of the constant low pH value of the mobile phase, in which only the protonated AMLH$^+$ is present. Besides this, chromatographic analysis did not allow for the complete description and continuous monitoring of the kinetic reaction. Spectrophotometric methods, like UV absorption, are able to monitor more accurately and continuously photodegradation kinetic processes in the lab, without interfering the progress of the reactions nor the formation of the species involved. In fact, MCR-ALS analysis of **D$_2$** allowed a better description of both kinetics and acid-base equilibria of the species involved. The augmentation of the UV spectrophotometric data with the UV-DAD chromatographic data removed the rank deficiency associated to MCR resolution of only spectrophotometric data, and allowed the evaluation of the correct number of involved species, enhancing the information provided by spectrophotometric monitoring. However, the structures and identification of the photoproducts was not possible only with the UV information.
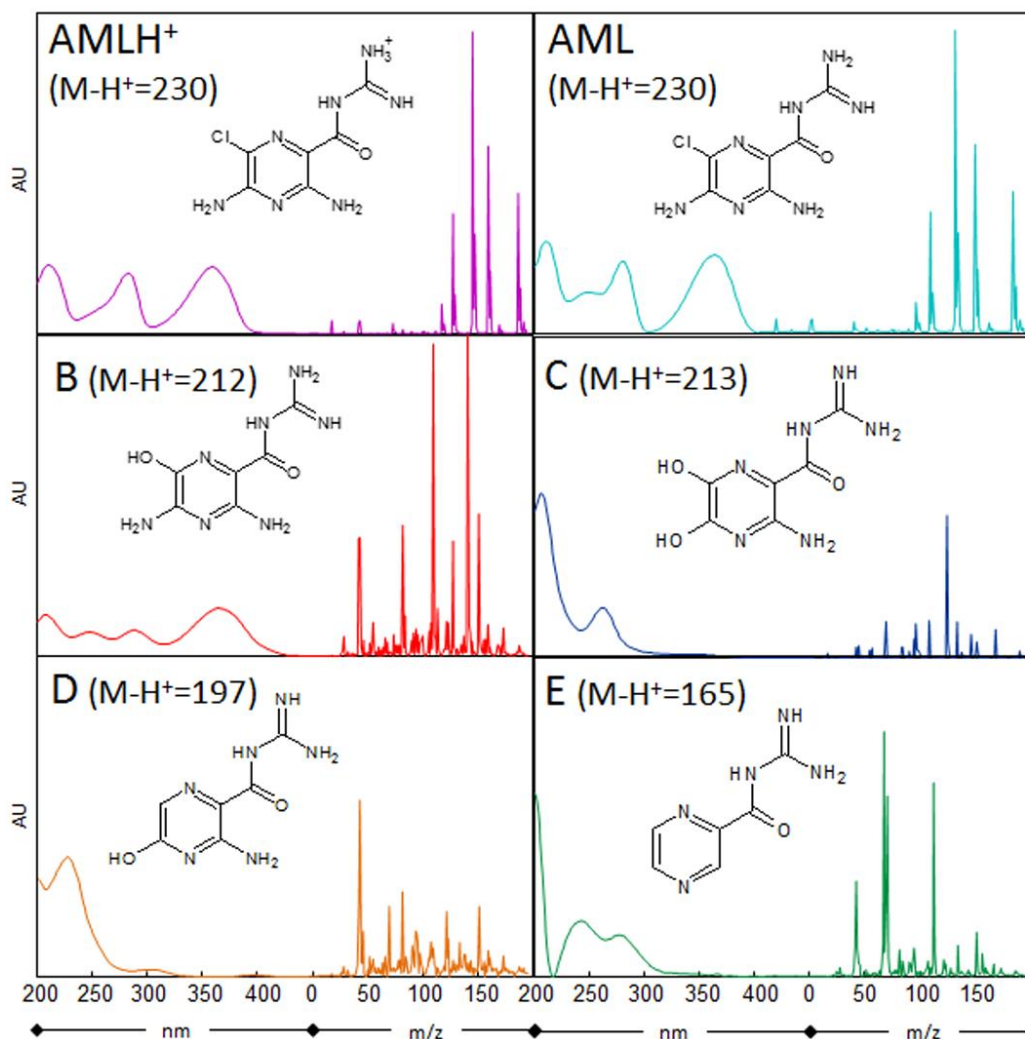
Figure 3.15 - Concentration profiles and pure spectra resolved by MCR-ALS analysis of the incomplete data multiset (D_{aug}), which includes UV titration, kinetic photodegradation and LC-DAD-MS experiments.

Figure 316 - DAD/MS spectra (S_{aug}^T) resolved by MCR analysis and related proposed structures.

As can be seen in figure 3.15, MCR-ALS analysis of the data multiset **D$_{aug}$**, including spectrophotometric and chromatographic data (both UV and MS), allowed the comprehensive description of the photodegradation of AML, providing simultaneously information about its kinetics, acid-base reactions and UV and LC-MS identification of the photoproducts. In accordance with these results, the proposed pathway for the AML photodegradation process is shown in figure 3.15, in which both acid-base species, AML and AMLH$^+$, and the formation of their corresponding photoproducts have been considered and properly described.

UV spectrophotometric kinetic data coupled to chromatographic data using DAD and MS detectors simultaneously joined the information from all experiments and from both analytical detection systems, UV and MS. In this data fusion procedure, UV absorbance data of chromatographic DAD provided the bridge between UV and MS spectra for all species involved in acid-base and kinetic experiments.

MCR-ALS analysis of the incomplete data multiset D_{aug} described the full AML photodegradation process by identifying four different photoproducts in a series of consecutive first-order reactions, with a possible pathway such as AML/AMLH$^+$>B>C>D>E (see figure 3.15). The pH was confirmed to influence the degradation pathway. In fact, species distribution of photodegradation experiments at pH 3, 7, 9 and 12 resulted to be different. Figure 3.16 shows UV and MS spectra of the different species resolved by MCR-ALS analysis are shown (S_{aug}^T matrix). MS spectra of the resolved species by MCR-ALS allowed the identification of the formed species and the postulation of the photodegradation mechanism taking place. Photodegradation of AML/AMLH$^+$ (m/z = 230, RT = 6.13 min) started with the photo-induced dechlorination and substitution of Cl group with an OH group on the heterocyclic ring (species B, m/z = 212, RT = 2.19 min), followed by the substitution of the NH$_2$ group with an OH group (species C, m/z = 213, RT = 4.01 min), loss of a molecule of water (species D, m/z = 197, RT = 2.87 min) and then the loss of OH and NH$_2$ groups from the heterocyclic ring (species E, m/z = 165, RT = 2.90 min) (De Luca et al., 2012; Calza et al., 2008). According to these results, proposed structures and mechanisms are displayed in Figures 3.15 and 3.16.

4. CONCLUSIONS.

This thesis is a research report achieved in the three years of PhD studies. In this period, I had the possibility to improve my know-how in pharmaceutical and analytical chemistry fields. My studies have been focused on the drug photostability studies by applying and developing new experimental and analytical procedures.

In the research stage in Spain, I had the opportunity to collaborate with the Professor Romà Tauler, head of one of the most important research group in chemometrics. During this period in the Barcelona CSIC center, I worked for the development of a new analytical procedure aimed to study in depth the kinetic degradation processes of pharmaceutical molecules.

As reported in the paragraph 3.1, I studied the application of a HPLC-DAD method to the thermal and photodegradation experiments, allowing to describe the degradation pathway of the anticancer lonidamine. The drug degradation process was shown to proceed with two different mechanisms when exposed to light or high temperature. Major degradation of the drug substance was found to occur in solution under forced irradiation to form photoproducts from debenzylation and decarboxylation whereas the heating of the drug solutions caused mainly decarboxylation.

In the paragraph 3.2, 3.3 and 3.4, new analytical methodologies I investigated drug photodegradation using spectrophotometric and chromatographic data. MCR-ALS resolution of the experimental data obtained in the photodegradation of melatonin and amiloride drugs showed the usefulness of these methods. The new multivariate data analysis approach described in this work, based on the use of a new version of the MCR-ALS algorithm, allowed the comprehensive study of both drug photodegradation processes. Application of the hard-modelling constrained HS-

MCR-ALS procedure, which takes into account the reaction mechanism and kinetic rate laws, permitted the practical elimination of any ambiguity, furnishing very reliable estimations of the rate constants of the ML kinetic process. These rate constant values were demonstrated to be strongly dependent on irradiance power. A significant increase of the rate constant of the degradation processes of melatonin was clearly observed with the increasing of the light power.

Amiloride study was more complex and the proposed strategy involved the simultaneous analysis of multiple experimental data sets from different analytical platforms, including UV spectrophotometric acid-base and kinetic data sets on one side, and DAD/MS-chromatographic data sets on the other side, all together combined in a hyper column- and row-wise augmented incomplete data set. Resolution of this incomplete multiset data allowed the simultaneous description of the kinetic photodegradation process of the drug at different pH values and the MS chromatographic identification of the photoproducts formed during the degradation of this drug.

The studied chemometric methodologies have thus demonstrated high power and ability to solve complex analytical systems and have the potential to be extended to the study of kinetic processes in any field of chemistry.

The works described in the PhD thesis have been published in:

1. M. De Luca, G. Ragno, G. Ioele, R. Tauler, Analytica Chimica Acta, 837 (2014) 31.

2. M. De Luca, R. Tauler, F. Oliverio, G. Ragno , Drug Testing and Analysis 5 (2013) 96.

3. G. Ioele, M. De Luca, G. Ragno, Anal. Methods, 5 (2013) 1715.

4. M. De Luca, G. Ioele, S. Mas, R. Tauler and G. Ragno, Analyst, 137 (2012) 5428.

Other research articles in period 2012-2014:

5. G. Ioele, M. De Luca, G. Ragno, Int. J. Pharm. Anal. 39 (2014) 2051-2740

6. G. Ioele, M. De Luca, L. Tavano, G. Ragno, Int. J. Pharmaceutics, 465 (2014) 284–290

7. M. De Luca, G. Ioele G. Ragno, J. Pharm. Biomed. Anal, 90 (2014) 35-43

8. M. Bassbasi, M. De Luca, G. Ioele, G. Ragno, A. Oussama, J. Food Comp. Anal. 33 (2014) 243-249.

9. G.Ioele, M.De Luca, G.Ragno, Future Med. Chem., 6 (2014)35-43.

10. M. De Luca, W. Terouzi, F. Kzaiber, G. Ioele, A. Oussama, G. Ragno, Int. J. Food Sci. Techn., 47 (2012) 1286-1292

11. G. Ioele, M. De Luca, G.P. Husson, G. Ragno, Eur. J. Water Quality, 43 (2012)43-52.

12. E. Dinç, G. Ragno, D. Baleanu, M. De Luca, G. Ioele, Spectrosc. Letters, 45 (2012) 337-343

13. G. Ioele, F. Oliverio, M. De Luca, G. Ragno, Curr. Pharm. Anal., 8 (2012)196-205

REFERENCES

E. Acar, D.M. Dunlavy, T.G. Kolda, M. Morup, Chemom. Intell. Lab. Syst. 106 (2011) 41.

K. Albert, M. Krucker, T. Glaser, A. Schefer, A. Lienau, D. Zeeb, Anal. Bioanal. Chem., 372 (2002) 25.

A. Albini, E. Fasani, Photochemistry of drugs: an overview and pratical problems. In A. Albini,E. Fasani (Ed), Drugs: photochemistry and photostability, The Royal Society of Chemistry, Cambridge, (1997) pp. 1.

M. Alier, M. Felipe, I. Hernández, R. Tauler, Anal. Bioanal. Chem. 399 (2011) 2015.

M. Alier, R. Tauler, Chemom. Intell. Lab. Syst. 127 (2013) 17.

M.C. Allowood, J.H. Plane. Int. J. Pharm. 31 (1986) 1.

D. Amadori, G.L. Frassineti, A. De Matteis, G. Mustacchi, A. Santoro, S. Cariello, M. Ferrari, O. Nascimben, O. Nanni, A. Lombardi, E. Scarpi, W. Zoli, Breast Cancer Res. Treat. 49 (1998) 209.

M. Amrhein, B. Srinivasan, D. Bonvin, M. M. Schumacher, Chemom. Intell. Lab. Syst., 33 (1996) 17.

N. H. Anderson and S. J. Byard, "Photostability of Drugs and Drug Formulations," (H. H. Tønnesen, Ed.), 137, New York: CRC Press (2004).

M. C. Andreazza Costa and A. C. Gaudio, J. Mol. Struc-Theochem. 394 (1997) 291.

V. Andrisano, C. Bertucci, A. Battaglia, V. Cavrini. J. Pharm. Biomed. Anal. 23 (2000) 15.

J. Axelrod, R.J. Wurtma. Adv. Pharmacol. 6 (1968) 157.

G. M. J. Beijersbergen Van Henegouwen, *Adv. Drugs Res.* 29 (1997) 79.

J.C. Berridge, P. Jones, A.S. Roberts-Mcintosh, J. Pharm. Biomed. Anal., 9 (1991) 597.

W.E. Bloch, B.L. Lokeshwar, S.M. Ferrell, N.L. Block, Prostate 24 (1994) 131.

C. Bottalico, G. Micelle, A. Guerrieri, F. Palmisano, V. Lorusso, M. De Lena, J. Pharm. Biomed. Anal. 13 (1995) 1349.

N. Bratchell. Chemometrics and Intelligent Laboratory Systems 6 (1989) 105.

R. Bro. Chemometrics and Intelligent Laboratory Systems 38 (1997) 149.

S.D. Brown, R. Tauler, B. Walczak. Comprehensive Chemometrics. Chemical and Biochemical Data Analysis, Elsevier, Amsterdam (2009).

P. Brugger, W. Marktl, M. Herold. Lancet, 245 (1995) 1408.

J. Cadet, C. Anselmino, T. Douki, and L. Voituriez, J. Photochem. Photobiol. B: Biol., 15 (1992) 277.

P. Calza, C. Massolino, G. Monaco, C. Medana, C. Baiocchi, J. Pharm. Biomed. Anal., 48 (2008) 315.

V. Chekulayev, I. Shevchuj, L. Chekulayeva, A. Kahru, J. Photochem. Photobiology B: Biology 41 (1997) 11.

P.J.G. Cornelissen, G.M.J. Beijersbergen van Henegouwen. Photobiol. 30 (1979) 337.

G. Corsi, G. Palazzo, C. Germani, P.S. Barcellona, B. Silvestrini, J. Med. Chem. 19 (1976) 778.

J. D. Coyle, R. R. Hill, and D. R. Roberts, "Light, Chemical Cange and Life: a Source Book in Photochemistry," Milton Keynes, UK: The Open University Press (1982).

M. Dahlitz, B. Alvarez, J. Vignau, J. English, J. Arendt, J.D. Parkes. Lancet. 137 (1991) 1121.

A. de Juan, E. Casassas, R. Tauler, Encyclopedia of Analytical Chemistry: Instrumentation and Applications,Wiley, New York, (2000).

A. de Juan, S. C. Rutan, M. Maeder, R. Tauler, Comprehensive Chemometrics; vol. 2, Elsevier, Amsterdam, (2009).

A. de Juan, R. Tauler. Crit. Rev. Anal. Chem. 36 (2006) 163.

A. de Juan, R. Tauler, J. Chemom. 15 (2001) 749.

A. de Juan, Y. Vander Heyden, R. Tauler, D.L. Massart. Anal. Chim. Acta 346 (1997) 307.

M. De Luca, G. Ioele, S. Mas, R. Tauler, G. Ragno, Analyst 137 (2012) 5428.

M. De Luca, S. Mas, G. Ioele, F. Oliverio, G. Ragno, R. Tauler, Int. J. Pharm., 386 (2010) 99.

M. De Luca, G. Ragno. Camo AS, Norway. www.camo.com/resources/application-notes.html, (2009).

H. D. Drew, in "Drugs: Photochemistry and Photostability" (A. Albini and E. Fasani, Eds.), 227, Cambridge: The Royal Society of Chemistry (1998).

J.H. Epstein, Photomedicine, in Smith, K.C. (Ed.), The Science of Photobiology. New York: Plenum Press (1989) 155.

J.E. Frederick, Photochem. Photobiol., 57 (1993) 175.

H. Gampp, M. Maeder, C.J. Meyer, A.D. Zuberbuehler. Anal. Chim. Acta. 193 (1987) 287.

R. Gargallo, R. Tauler, F. Cuesta-Sanchez, D.L. Massart. Trends Anal. Chem. 15 (1995) 279.

M. Garrido, M.S. Larrechi, F.X. Rius, R. Tauler. Chemom. Intell. Lab. Syst. 76 (2005) 111.

D.M. Gates, Science, 151 (1966) 523.

M.T. Gatto, B. Tita, M. Artico, L. Saso, Contraception 65 (2002) 277.

P.J. Gemperline. Anal. Chem. 71 (1999) 5398.

G.H. Golub, C.F. Van Loan. Matrix Computations, 2nd ed., The John Hopkins University Press, London (1989).

J.V. Greenhill, In: W.H. Horspool, and P.S. Song, Handbook of organic photochemistry and photobiology, CRC Press, Boca Raton, (1995) p. 83.

L.I. Grossweiner, Photophysics, in Smith, K.C. (Ed.), (1989)

G. Hanrahan. Environmental chemometrics. Principles and modern applications. CRC Pres, Taylor & Francis Group (2009).

A. Hatipoglu and Z. Çinar, *J. Mol. Struc-Theochem.* 631 (2003) 189.

B. Hemmateenejad, K. Javidnia, M. Saeidi-Boroujeni. J. Pharm. Biomed. Anal. 47 (2008) 625.

P. Helboe, "Drugs: Photochemistry and Photostability" (A. Albini and E. Fasani, Eds.), 243, Cambridge: The Royal Society of Chemistry (1998).

E. J. Hixson, J. A. Burdershaw, E. P. Denine, and S. D. Harrison, Toxicol. Appl. Pharmacol. 47 (1979) 359.

B. Hemmeteenejad, R. Miri, M. Akhond, and M. Shamsipur, Chemometr. Intell. Lab. 64 (2002) 91.

R.C. Henry, B.M. Kim. Chemom. Intell. Lab. Syst. 8 (1990) 205.

P.K. Hopke, Comprehensive Chemometrics: Chemical and Biochemical Data Analysis, Ed. Elsevier (2009).

W. H. Horspool and P. S. Song, "CRC Handbook of Organic Photochemistry and Photobiology," Boca Raton, FL: CRC Press (1995).

ICH Q1B, Photostability testing of new drug substances and products, Fed. Reg., 62, (1991) 27115.

G. Ioele, E. Cione, A. Risoli, G. Genchi, and G. Ragno, Int. J. Pharm. 293 (2005) 25.

M. Isidori, M. Lavorgna, A. Nardelli, A. Parrella, L. Previtera, M. Rubino, Sci. Total. Environ. 348 (2005) 93.

S. Ivana, Z. Ljiljana, Z. Mira, J. Chromatogr. A. 1119 (2006) 209.

A. Izquierdo-Ridorsa, J. Saurina, S. Hernadez-Cassou, R. Tauler, Chemom. Intell. Lab. Syst., 38 (1997) 183.

J. Jaumot, R. Gargallo, A. de Juan, R. Tauler, Chemom. Intell. Lab. Syst. 76 (2005) 101.

K. Javidnia, B. Hemmateenejad, R. Miri, M. Saeidi-Boroujeni, J. Pharm. Biomed. Anal., 46 (2008) 597.

W. Kessler, R.W. Kessler. Anal. Bioanal. Chem. 384 (2006) 1087

B.M. Kim, R.C. Henry. Chemom. Intell. Lab. Syst. 49 (1999) 67.

D. M. Kochar, J. D. Penner, and C. I. Tellone, Teratogen. Carcin. Mut. 4 (1984) 377.

H.L. Koh, W.P. Yau, P.S. Ong, A. Hegde, Drug Discov. Today, 8 (2003) 889.

J. Kopecky, "Organic Photochemistry: A Visual Approach," New York: VCH (1992)

B.K. Lavine, Comprehensive Chemometrics: Chemical and Biochemical Data Analysis, Ed. Elsevier (2009).

R. Leclaire, J.G. Besner, P. Band, S. Mailhot, P. Gervais, A. De Sanctis, M. Deschamps, J. Chromatography B: Biomedical Sciences and Applications 277 (1983) 427.

D. Leger, M. Laudon, N. Zisapel. Am. J. Med. 116 (2004) 91.

M. N. Leger, P. D. Wentzell, Chemom. Intell. Lab. Syst., 62 (2002) 171.

A. A. Lev, I. O. Veinberg, Dokl. Biol. Sci., 399 (2004) 415.

Y. N. B. Li, D. E. Moore, B. N. Tattam, Int. J. Pharm., 183 (1999) 109.

A. Malik, R. Tauler, Anal Chim Acta, 2013, doi: 10.1016/j.aca.2013.07.047.

M. Maeder,Y. M. Neuhold, Practical data analysis in chemistry, Elsevier Ltd., Netherlands, 2007.

M. Maeder, A.D. Zuberbuhler. Anal. Chem. 62 (1990) 2220.

L. Magno, F. Terraneo, F. Bertoni, M. Tordiglione, D. Bardelli, M.T. Rosignoli, G.B. Ciottoli, Int. J. Radiat. Oncol. Biol. Phys. 29 (1994) 45.

I. A. Magnus, Dermatological Photobiology, Blackwell, London (1977).

R. Manne. Chemom. Intell. Lab. Syst. 27 (1997) 89.

S. Mas., A. de Juan, S. Lacorte, R. Tauler. Anal. Chim. Acta 618 (2008) 18.

D.L. Massart, B.G.M. Vandeginste, L.M.C. Buydens, S. De Jong, P.J. Lewi, J. Smeyers-Verbeke, Handbook of Chemometrics and Qualimetrics, Part A. Amsterdam. Elsevier Science (1997).

A. Mohammadi, I. Haririan, N. Rezanour, L. Ghiasi, R.B. Walker, J. Chromatogr. A 1116 (2006) 153.

D. E. Moore, "Photostability of Drugs and Drug Formulations," (H. H. Tønnesen, Ed.), New York: CRC Press (2004) 41.

L. Norgaard, C. Ridder, Chemom. Intell. Lab. Syst., 23 (1994) 107.

S.R. Pandi-Perumal, I. Trakht, V. Srinivasan, D.W. Spence, G.J.M. Maestroni, N. Zisapel, D.P. Cardinali. Prog. Neurob. 85 (2008) 335.

H. Pelicano, D.S. Martin, R.H. Xu, P. Huang, Oncogene 25 (2006) 4633.

E. Peré-Trepat, A. Ginebreda, R. Tauler, Chemom. Intell. Lab. Syst. 88 (2007) 69-83.

L. Periolia, V. Ambrogia, B. Bertinia, M. Riccia, M. Nocchettib, L. Latterinib, and C. Rossia, Eur. J. Pharm. Biopharm. 62 (2006), 185.

G. Ragno, G. Ioele, M. De Luca, A. Garofalo, F. Grande, A. Risoli, J. Pharm. Biomed. Anal. 42 (2006) 39.

G. Ragno, A. Risoli, G. Ioele, E. Cione, M. De Luca, J. Nanosc. Nanotech., 6 (2006a) 2979.

G. Ragno, A. Risoli, G. Ioele, M. De Luca, Chem. Pharm. Bull., 54(6) (2006b) 802.

R. O. Rahn, L. C. Landry, and W. L. Carrier, Photochem. Photobiol. 19 (1974) 75.

R. Rajko, K. J. Istvan, *J.Chemom.*, 19 (2005) 448.

G. Robustelli della Cuna and P. Pedrazzoli, Semin. Oncol. 18 (1991) 18.

R. Rosso, D. Amoroso, G. Gardin, L. Miglietta, T. Guido, M. Pace, L. Repetto, P. Pronzato, Semin. Oncol. 18 (1991) 62.

C. Ruckebusch and L. Blanchet, Analytica Chimica Acta 765 (2013) 28.

E. Sánchez, B.R. Kowalski, Analytical Chemistry 58 (1986) 496.

E. Sánchez, B.R. Kowalski. Journal of chemometric, 4 (1990) 29.

I. Shevchuk, V. Chekulayev, J. Moan, K. Berg, Int. J. Cancer 67 (1996) 791.

B. Silvestrini, Semin. Oncol. 18 (1991) 2.

B. Silvestrini, G. Palazzo, M. De Gregorio, Prog. Med. Chem. 21 (1984) 110.

A. Smilde, R. Bro, P. Geladi, Multi-Way Analysis: Applications in the Chemical Sciences, Wiley, West Sussex, (2004).

S. Singh, B. Singh, R. Bahuguna, L. Wadhwa, R. Saxena, J. Pharm. Biomed. Anal. 41 (2006) 1037.

D.A. Skoog, D.M. West. Fundamentals of analytical chemistry, Brooks/Cole, Belmont, (CA) USA (2004).

J.V. Sweedler, Anal. Bioanal. Chem., 373 (2002) 321.

P. Song and K. J. Tapley, Photochem. Photobiol. 29 (1979) 1177.

J. Suykens, Comprehensive Chemometrics: Chemical and Biochemical Data Analysis, Ed. Elsevier (2009).

L. Tao, Z. Xian-Cheng, Y. Xiu-Cen, H. Ning, L. Cheng-Rong, L. Lin-Li. J. Chem. 23 (2005) 1090.

R. Tauler. Anal. Chim. Acta 595 (2007) 289.

R. Tauler, Chemometrics and Intelligent Laboratory Systems 30 (1995) 133.

R. Tauler. J. Chemom. 15 (2001) 627.

R. Tauler, Chemom. Intell. Lab. Syst. 30 (1995) 133.

R. Tauler, A. Izquierdo-Ridorsa, E. Casassas. Chemom. Intell. Lab. Syst. 18 (1993) 293.

R. Tauler, M. Maeder, A. de Juan, Comprehensive Chemometrics, Vol.2, Elsevier, (2009).

R. Tauler, I. Marqués, E. Casassas, J. Chemom. 12 (1998) 55.

R. Tauler, A.K. Smilde, B.R. Kowalski. J. Chemom. 9 (1995) 31.

H. H. Tønnesen, "Photostability of Drugs and Drug Formulations", New York: CRC Press, 2004

H. H. Tønnesen, Int. J. Pharm. 225 (2001) 1.

L.R. Tucker. Psychometrica 31 (1966) 279.

C. Vetuschi, G. Ragno, L. Baiocchi, P. Ridolfi, Spectr. Lett. 22 (1989) 375.

C. Vetuschi, G. Ragno, Anal. Lett. 22 (1989) 19.

H. de Vries and G. M. J. Beijersbergen van Henegouwen, J. Photoch. Photobio. B 43 (1998) 217.

D. G. Vidt, Pharmacotherapy, 1 (1981) 179.

P. D. Wentzell, J. Wang, L. F. Loucks, K. M. Miller, Can. J. Chem., 76 (1998) 1144.

W. Windig, J. Guilment. Anal. Chem. 63 (1991) 1425.

S. Wold, J. Cheney, N. Kettaneh, C. McCready, Chemometrics Intell. Lab. Syst., 84 (2006) 159.